Calm on the surface, dynamic on the inside. Molecular homeostasis in response to regulatory and metabolic perturbation of *Anabaena* sp. PCC 7120 nitrogen metabolism

Giorgio Perin[1], Tyler Fletcher[2], Virag Sagi-Kiss[3], David C. A. Gaboriau[4], Mathew R. Carey[3], Jacob G. Bundy[3], Patrik R. Jones[1*]

1. Department of Life Sciences, Imperial College London, London, UK
2. Complex Carbohydrate Research Center and Department of Chemistry, University of Georgia, Athens, Georgia, USA
3. Department of Metabolism, Digestion and Reproduction, Imperial College London, London, UK
4. Facility for Imaging by Light Microscopy, NHLI, Imperial College London, London, UK

* Corresponding author. E-mail: p.jones@imperial.ac.uk

Abstract

Nitrogen is a key macro-nutrient required for the metabolism and growth of biological systems. Although multiple nitrogen sources can serve this purpose, they are all converted into ammonium/ammonia as a first step of assimilation. It is thus reasonable to expect that molecular parts involved in the transport of ammonium/ammonia across biological membranes (i.e. catalysed by AMT transporters) connect with the regulation of both nitrogen and central carbon metabolism. In order to test this hypothesis, we applied both (1) genetic (i.e. *Δamt* mutation) and (2) environmental treatments to a target biological system, the cyanobacterium *Anabaena sp.* PCC 7120. Cyanobacteria have a key role in the global nitrogen cycle and thus represent a useful model system. The aim was to both (1) perturb sensing and low-affinity uptake of ammonium/ammonia and (2) induce multiple inner N states, followed by targeted quantification of key proteins, metabolites and enzyme activities, with experiments intentionally designed over a longer time-scale than the available studies in literature. We observed that the absence of AMT transporters triggered a substantial response at a whole-system level, affecting enzyme activities and the quantity of both proteins and metabolites, spanning both N and C metabolism. Moreover, the absence of AMT transporters left a molecular fingerprint indicating N-deficiency even under N replete conditions (i.e. greater GS activity, lower 2-OG content and faster nitrogenase activation upon N deprivation). Contrasting with all of the above dynamic adaptations was the striking near-complete lack of any externally measurable phenotype (i.e. growth, photosynthesis, pigments, metabolites). We thus conclude that this species evolved a highly robust and adaptable molecular network to maintain homeostasis, resulting in substantial internal but minimal external perturbations. The analytical data highlights several internal adaptations, including increased N assimilation (i.e. greater GS activity) and nitrogenase activity (i.e. faster activation upon N deprivation) together with altered amino acids metabolism, as indicated by changes in Gln, Glu and 2-OG, indicating an altered C/N balance. The analyses provides evidence for an active role of AMT transporters in the regulatory/signalling network of N metabolism in this biological system, and the existence of a novel fourth IF7A-independent regulatory mechanism controlling GS activity.

Keywords

46 *Anabaena sp. PCC 7120*; AMT transporters; Nitrogen metabolism; Systems biology; Homeostasis
47 control

Introduction

Cyanobacteria are a group of morphologically diverse oxygenic photosynthetic bacteria (Singh & Montgomery, 2011) almost ubiquitous to every habitat on Earth, from hot springs to Antarctic rocks (Percival & Williams, 2013). They are often found as integral members of complex ecosystems representing all three domains of life (Adams & Duggan, 2008; Adams *et al*, 2013) where they contribute to whole ecosystem functionality by photosynthesis-driven assimilation of nutrients. One of the key nutrients they assimilate and provide to the (local) ecosystem is nitrogen (N), an essential building block for amino and nucleic acid biosynthesis. Cyanobacteria have a variety of complementary N assimilatory pathways, including ammonium [NH_4^+, (Montesinos *et al*, 1998)], nitrate [NO_3^-, (Omata *et al*, 1993)] nitrite [NO_2^-, (Bird & Wyman, 2003)] and urea (Valladares *et al*, 2002), and have a key role in the global nitrogen cycle (Flores & Herrero, 2005). Some genera even use amino acids [e.g. arginine and glutamine (Montesinos *et al*, 1997)] or directly fix atmospheric nitrogen [biological nitrogen fixation (BNF), (Herrero *et al*, 2001)], globally contributing 200 million tonnes of fixed N per year (Rascio & La Rocca, 2013). Cyanobacteria are also involved in symbiotic associations, with reduced carbon delivered to cyanobacteria in order to sustain BNF (Backer *et al*, 2018). An example of such symbiotic associations is the aquatic fern *Azolla caroliniana*, which receives fixed N from a filamentous cyanobacterium (*Anabaena azollae*) hosted in the ovoid cavities of the plant's leaves (Lechno-Yossef & Nierzwicki-Bauer, 2005).

In its free-living form, this cyanobacterium makes a significant contribution to the carbon and nitrogen economy of multiple ecosystems (Kellar & Goldman, 1979). *Anabaena sp. PCC 7120* (henceforth 7120) is an isolated strain showing high genome sequence similarity with *Anabaena azollae* and is commonly used as a model organism to investigate cyanobacterial N-fixation (Herrero *et al*, 2016). As nitrogenases are oxygen-sensitive, photosynthesis-driven BNF calls for spatial and/or temporal separation between the metabolic pathway fuelling energy/carbon inputs (i.e photosynthesis) and N -fixation (Fig. 1). Under diazotrophic conditions, 7120 differentiates 5-10% of its cells into specialised N -fixing heterocysts, following a highly regulated developmental pattern [i.e. a single heterocyst every 10-20 cells (Kumar *et al*, 2010)]. Heterocysts undergo a deep metabolic and structural remodelling to enable efficient N fixation (Golden & Yoon, 1998). The oxygen-evolving photosystem II (PSII) is dismantled, carbon fixation is avoided, photorespiratory activity is increased during differentiation (Valladares *et al*, 2007) and cells are surrounded by a thicker cell envelope [through the deposition of two additional envelope layers, i.e. an inner glycolipids and an outer polysaccharides layer (Nicolaisen *et al*, 2009)] than the vegetative cells, providing the required microoxic environment for N fixation activity (Kumar *et al*, 2010)(Fig. 1).

Heterocysts and vegetative cells have complementary metabolism, with the former providing fixed nitrogen and the latter returning reduced carbon needed to sustain BNF (Malatinszky *et al*, 2017). This metabolic exchange and associated networks (summarised in Fig. 1) are most likely carefully coordinated in order to ensure organism-level homeostasis (Mullineaux *et al*, 2008). The question is, how does this molecular coordination take place?

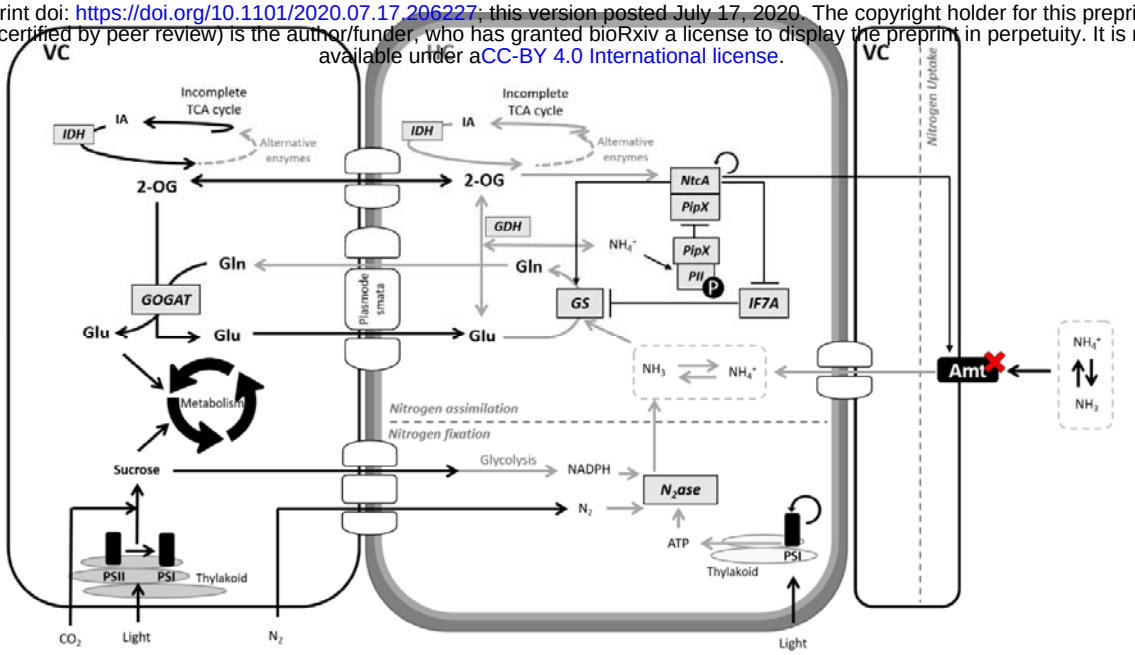

Figure 1. Schematic overview of major molecular players regulating N metabolism and the metabolic interaction between heterocysts (HC) and vegetative (VC) cells in Anabaena sp. PCC 7120, in diazotrophic conditions. *Nitrogenase (N_2ase) fixes one molecule of atmospheric N_2 into two molecules of NH_3 in heterocysts (Inomura et al, 2017), using reducing power (NADPH) from the catabolism of carbon -compounds (sucrose) photosynthesised in vegetative cells (Cumino et al, 2007; Nürnberg et al, 2015) and energy (ATP) from the residual photosynthetic activity in heterocysts [i.e. cyclic electron flow around photosystem I (PSI), (Cardona & Magnuson, 2010)]. NH_3 is then assimilated through glutamine synthetase (GS) via the amidation of glutamate (Glu) to glutamine (Gln) (Forchhammer & Selim, 2019). GS activity is controlled through posttranslational inactivation (Bolay et al, 2018) by IF7A (Galmozzi et al, 2010). Glutamate dehydrogenase (GDH) marginally contributes to the assimilation flux of fixed N, catalysing the reversible conversion of 2-oxoglutarate (2-OG) to Glu. Subsequently, in vegetative cells (Martín-Figueroa et al, 2000), glutamine oxoglutarate aminotransferase (GOGAT) catalyses the transfer of the amine group from Gln to 2-OG, generating two molecules of Glu. As N metabolism spans different cell types, a coordinated exchange of metabolites (i.e. sucrose, Gln, Glu and 2-OG) between vegetative cells and heterocysts via septal junctions [plasmodesmata (Mullineaux et al, 2008)] is required to maintain metabolic homeostasis. 2-OG is also a metabolic intermediate of the tricarboxylic acid (TCA) cycle [synthesised from isocitric acid (IA) by isocitrate dehydrogenase (IDH)], thus connecting N and C metabolism at a central point. N metabolism homeostasis is controlled by a molecular network, including the proteins NtcA, PipX and PII. When external N is available, PII is not phosphorylated and it sequesters PipX, preventing its biding to NtcA and consequently its activation. When N is limiting, PII is phosphorylated, freeing PipX, which ultimately binds and activates NtcA* (Flores & Herrero, 2005). *The red cross indicates the knock-out (KO) mutant Δamt used in this work* (Paz-Yepes *et al*, 2008). *Major molecular players targeted in this work are highlighted by a grey square or in bold, respectively for proteins and metabolites.*

In many organisms, including 7120, N metabolism is orchestrated by a complex signalling network with the likely aim to balance the cellular C/N ratio (Forchhammer & Selim, 2019). N and C metabolism are in fact tightly coupled as (1) the two elements are the most abundant in living organisms, calling for coordination to avoid metabolic inefficiencies, and (2) N assimilation depends on the availability of C skeleton, with shortage or oversupply strongly affecting the metabolism of N (Zhang *et al*, 2018). Therefore, a properly balanced N and C metabolism is necessary for optimal growth and different levels of regulation exist to control uptake and assimilation efficiencies of both chemical species. When the C source (i.e. CO_2 in case of phototrophic metabolism) is not limiting,

the regulatory mechanisms controlling C/N balance depend on both the abundance and the nature of the N sources available to the cell. Although cyanobacteria can use multiple N sources, including NH_4^+, intracellularly they are all converted to NH_4^+, the most reduced and energetically favourable N source (Robinson, 2017). Ammonia translocation across biological membranes is actively driven by AMT transporters that belong to a family of permeases widely distributed in living organisms (Javelle *et al*, 2007), or through passive diffusion if the external pH pushes the equilibrium towards the uncharged form (NH_3, ammonia). 7120 bears a gene cluster including three *amt* genes, namely *amt4*, *amt1* and *amtB* (Paz-Yepes *et al*, 2008). In this work, we used a knock-out (KO) mutant of the whole gene cluster in 7120 [henceforth Δamt, (Paz-Yepes *et al*, 2008)] to perturb both the sensing of external N and low-affinity uptake of $NH4^+$, with the aim to investigate how a N_2-fixing cyanobacterium responds to perturbation of N-metabolism at a whole-system level. Although several genes and proteins in 7120 have been individually studied previously (Flores & Herrero, 2005; Forchhammer & Selim, 2019), it is difficult to make over-arching conclusions on the regulatory system, also as cyanobacteria differ substantially relative to heterotrophic bacteria (Reitzer, 2003; Bolay *et al*, 2018). The aim of this work is also to enhance our understanding that contributes towards the practical goal of eventually rerouting N -metabolism for biotechnological purposes (Perin *et al*, 2019).

Results

Amt transporters are not required to support growth of 7120 under constant laboratory conditions but play a role in N metabolism

Phototrophic growth of 7120 WT and Δ*amt* strains was carried out in media with different N sources (NO_3^-, N_2 and NH_4^+) at saturating CO_2 (i.e. 1%), in order to avoid C limitation. Such conditions are expected to vary the internal C/N balance by modifying the abundance and nature of the N source. The Δ*amt* mutant did not display any growth phenotype with respect to the parental strain, regardless of the N source (Fig. 2A), confirming that the whole *amt* cluster is not necessary to support growth of 7120 under the tested laboratory conditions (Paz-Yepes *et al*, 2008).

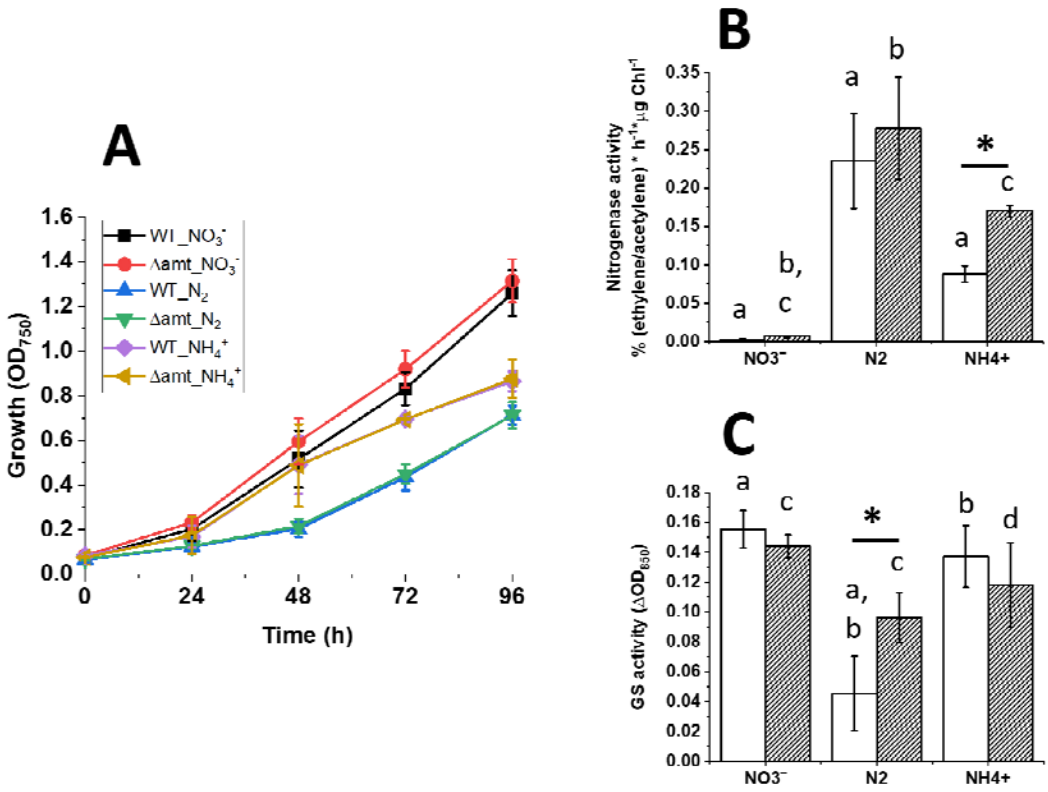

Figure 2. Growth of 7120 WT and Δamt strains with different N sources. *The two strains were cultivated in different N sources for 96 h. Growth (A) was monitored over the course of the whole experiment, whilst Nitrogenase activity (B) and GS activity (C) were measured after 96 h in such cultivation conditions. Data are indicated as average ± SD of 6 biological replicates. Statistically significant differences between WT (white bars) and Δamt (striped bars) are indicated with an asterisk, whilst the same alphabet letter indicates statistically significant differences for the same strain in different growth conditions (one-way ANOVA, p-value < 0.05).*

Growth in atmospheric N_2 lags behind both NO_3^- and NH_4^+, with cells taking ~48 hours to fully switch to atmospheric N_2 fixation. Growth in NH_4^+ shows two distinct modes, as indicated by the specific growth rate (Supplementary Fig. S2), suggesting that 5 mM NH_4^+ is not enough to support maximal growth (i.e. growth in NO_3^- in this experiment) over the whole experimental time frame, and that it likely runs out after ~48 hours (Fig. 2A). The nitrogenase activity, measured after 96 hours, confirms that 5 mM NH_4^+ runs out over the course of the experiment, triggering diazotrophic growth (Fig. 2B).

Moreover, the lower nitrogenase activity with respect to N_2 conditions highlights that cells in $NH4^+$ media, at the time of sampling, are in a transitory phase before reaching the maximal N fixation potential. Interestingly, in $NH4^+$ media, the Δ*amt* strain shows a higher nitrogenase activity per unit of chlorophyll (Chl) than the parental strain, although that does not result in an improvement in growth, suggesting possible compensatory modifications in the following metabolic steps (e.g. N assimilation). After 96 h, GS activity, a (supposed) central player in N metabolism in this organism (Bolay *et al*, 2018), is also affected by the mutation (as in the case of fully diazotrophic conditions (N_2) in which Δamt strain shows a greater N assimilation activity than the WT, see Fig. 2C). Moreover, when both strains are grown in N_2, GS activity is overall lower than in the other two growth conditions. The collective data indicated that the loss of AMT resulted in no phenotypic change, but that N-metabolism had adjusted, presumably to maintain homeostasis, raising the following question: how extensive was this adaption and what molecular players were involved?

In 7120, GS is regulated both transcriptionally and post-translationally, according to the C/N status of the cell (Bolay *et al*, 2018). The abundance of the protein is transcriptionally controlled and changes according to the N source(s) as observed in the WT strain, but not in Δ*amt* (Fig. 3A).

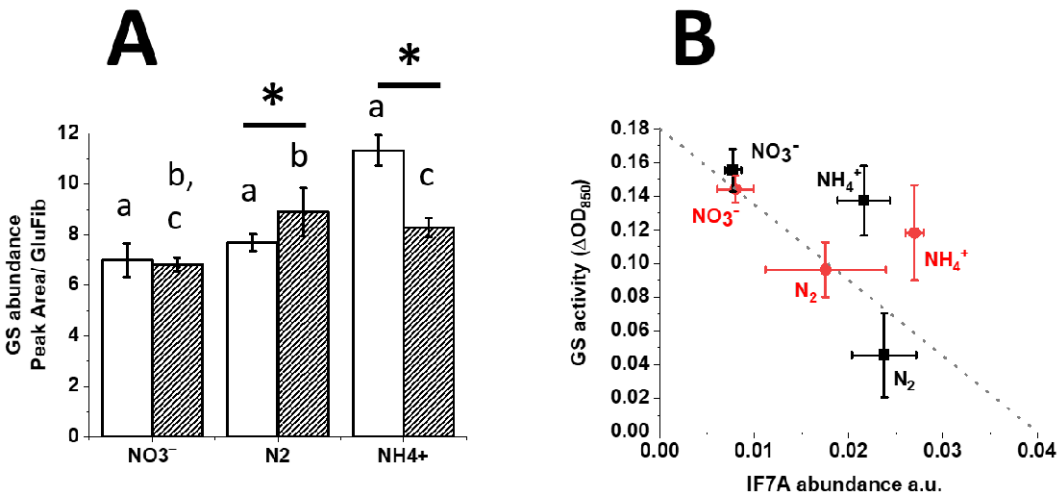

Figure 3. GS abundance and correlation between GS activity and IF7A amount for 7120 WT and Δamt strains, after 96 h in the growth conditions of figure 2A. IF7A quantification data are reported in supplementary Fig. S3. Data are indicated as average ± SD of 6 biological replicates. *Statistically significant differences between WT (white bars and black squares) and Δamt (striped bars and red circles) are indicated with an asterisk, whilst the same alphabet letter indicates statistically significant differences for the same strain in different growth conditions (one-way ANOVA, p-value < 0.05).*

The abundance of GS (Fig. 3A) does not reflect its measured activity (Fig. 2C). GS activity is known to be controlled by covalent binding of the inactivation factor IF7A, in response to the C/N balance of the cell (Galmozzi *et al*, 2010). As shown in Fig. 3B, in the WT strain, GS activity broadly displays a negative correlation with the amount of the inactivation factor IF7A, as expected. There is no linear correlation for either of the strains across different N sources, however, suggesting other molecular

players also contribute to the regulation of GS activity in this organism. The absence of AMT transporters has an effect on the IF7A/GS activity relationship (Fig. 3B). In N replete conditions (NO_3^-), there is no difference between the two strains, whilst under the two other N deplete conditions, the deletion of *amt* results in a divergence between the two strains (Fig. 3B). The genetic and environmental treatments affect GS activity through a combined variation in both GS and IF7A abundance (Fig. 3A and supplementary Fig. S3). In particular, it is worth noting that Δ*amt* retains GS activity even if the amount of IF7A changes, supporting the idea that other regulatory players also may be involved. Based on the available data, we hypothesised that AMT transporters are directly or indirectly involved in the regulation of GS activity during the switch towards diazotrophic conditions in 7120, as already observed in the purple bacterium *Rhodobacter capsulatus* (Yakunin & Hallenbeck, 2002).

Amt transporters regulate N metabolism homeostasis in 7120

In order to test this hypothesis, the internal metabolic changes taking place in 7120 WT and Δ*amt* during the transition from N replete to deplete conditions were followed by combining physiological data with targeted proteomic and metabolomic quantification of molecular players known to be involved in the regulation of N metabolism in 7120 (Fig. 1). Both WT and Δ*amt* strains were cultivated in $BG11_0$ supplemented with 5 mM NH_4^+. The concentration of ammonium/ammonia in the media and cell growth was monitored over time (Fig. 4A). Four different time points were chosen to investigate the physiological and metabolic status of the cells [i.e. NR (N replete conditions), ND1, ND2 and ND4 (1, 2 and 4 days, respectively, after N depletion), corresponding to 24, 72, 96 and 144 h from the start of the experiment]. Former studies in 7120 mainly focused on the first 24 h after N deprivation (Galmozzi *et al*, 2010; Valladares *et al*, 2011), as heterocyst differentiation is expected to occur within such time frame (Valladares *et al*, 2011). Here, instead, we opted for an extended sampling protocol in order to complement the information already available in literature with the knowledge of the metabolic/proteomic adjustments happening over a longer time-scale.

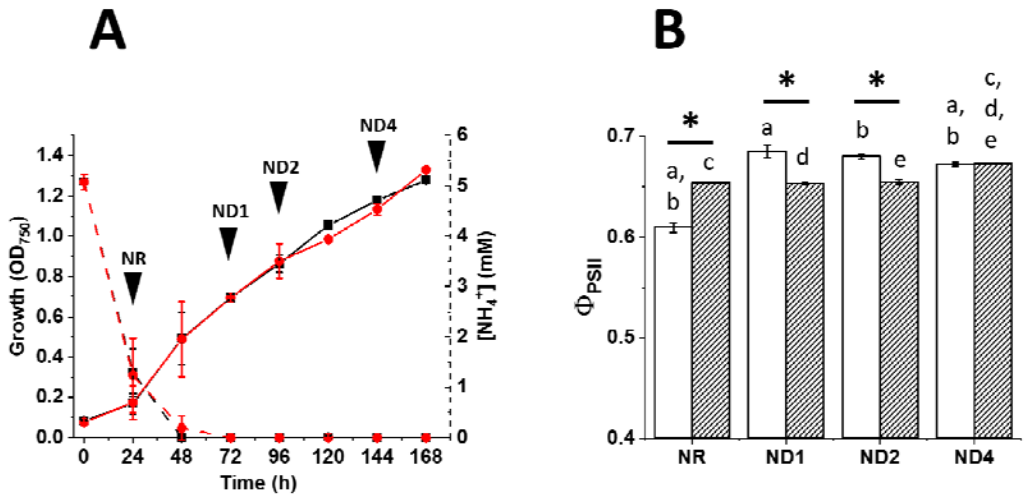

Figure 4. Growth, ammonium/ammonia consumption (A) and maximal photosynthetic efficiency [(Φ_{PSII}), (B)] monitoring for 7120 WT and Δamt strains in $BG11_0$ + 5 mM NH_4^+. *In A., black and red dashed lines indicate ammonium/ammonia concentration over time for 7120 WT and Δamt strains, respectively. Cultures were*

sampled at four time points over the course of the experiment [NR (Nitrogen Replete), ND1, ND2 and ND4, respectively 1, 2 and 4 days after Nitrogen Deprivation]. Data are indicated as average ± SD of 6 biological replicates. Statistically significant differences between WT (black squares and white bars) and Δamt (red circles and striped bars) are indicated with an asterisk, whilst the same alphabet letter indicates statistically significant differences for the same strain in different growth conditions (one-way ANOVA, p-value < 0.05).

The absence of the whole *amt* cluster does not affect the ammonium/ammonia consumption rate, indicating the diffusion of ammonia is enough to sustain growth in 7120, under the tested experimental conditions (Fig. 4A). Moreover, ammonium/ammonia in the medium is fully depleted after 48 h (Fig. 4A), confirming 5 mM NH_4^+ is not enough to support maximal growth in 7120 over a 96 h-long experiment (Fig. 2A). Over the course of the experiment, both strains mostly showed a stable pigment content, suggesting the switch towards diazotrophic conditions does not unbalance the overall N status of the cell (Table 1).

Table 1. Pigment content of WT and Δamt strains during the switch from N replete to deplete conditions. *Cultures were sampled at four time points over the course of the experiment [NR (Nitrogen Replete), ND1, ND2 and ND4, respectively 1, 2 and 4 days after Nitrogen Deprivation], according to Fig. 4A. Data are indicated as average ± SD of 6 biological replicates. Statistically significant differences between WT and Δamt are indicated with an asterisk, whilst the same alphabet letter indicates statistically significant differences for the same strain in different growth conditions (one-way ANOVA, p-value < 0.05).*

Chl content (µg/OD_{750})	WT	Δamt
NR	13.36 ± 0.49 ^{a}	14.14 ± 0.55 ^{d}
ND1	13.41 ± 0.18 ^{b}	13.38 ± 0.41 ^{e}
ND2	12.37 ± 0.37 ^{*,a,b,c}	14.26 ± 0.27 ^{*,e}
ND4	14.49 ± 0.72 ^{*,c}	16.13 ± 0.41 ^{*,d,e}
Car content (µg/OD_{750})		
NR	5.78 ± 0.2 ^{*,a}	4.73 ± 0.22 ^{*,c}
ND1	4.84 ± 0.05 ^{a,b}	4.7 ± 0.13 ^{d}
ND2	4.49 ± 0.12 ^{a,b}	4.76 ± 0.11 ^{e}
ND4	5.54 ± 0.29 ^{b}	5.86 ± 0.18 ^{c,d,e}

Chl/Car		
NR	2.31 ± 0.005 *,a	2.99 ± 0.02 *,c
ND1	2.77 ± 0.01 *,a	2.85 ± 0.01 *,c,d
ND2	2.75 ± 0.01 *,b	2.99 ± 0.01 *,d
ND4	2.61 ± 0.009 *,a,b	2.75 ± 0.01 *,c,d

However, the Δ*amt* strain shows a greater Chl/Car ratio, mainly achieved through the accumulation of a higher Chl content than the parental strain (Table 1). This effect on the pigment composition has also a consequence on the photosynthetic performances. The photosynthetic activity in the parental strain changes over the course of the experiment, whilst in Δ*amt* it is more stable (Fig. 4B). Moreover, the mutant shows a higher photosynthetic efficiency than WT in N replete conditions, while the difference reverses both after 24 and 48 h under N deprivation conditions and ultimately disappears after 96 h (Fig. 4B). Given that the Δ*amt* mutation does not trigger any growth phenotype, whilst there are substantial changes to both photosynthesis and N metabolism, we hypothesised that the deletion of the whole *amt* cluster is in fact triggering a whole cell metabolic response in order to maintain homeostasis.

In order to validate the two unanswered hypotheses, we investigated the N metabolism of 7120 more closely, targeting the same proteins and enzymatic reactions as above, but this time measured in the same time intervals as indicated in Fig. 4A. Both WT and Δ*amt* strains activate N fixation (Fig. 5A) as a consequence of ammonium/ammonia deprivation (Fig. 4A). The Δ*amt* strain shows a higher nitrogenase activity than the parental strain in both ND1 and ND2, indicating a faster response to N deprivation than the parental strain (Fig. 5A). Abundance of NifK and NifD, encoding for α and β subunits of nitrogenase, is higher in the mutant strain (Fig. 5B and 5C, respectively), suggesting increased N fixation activity depends at least in part on a greater accumulation of the protein complex, given also the number of heterocysts over the course of the experiment is not affected by the mutation (Supplementary Fig. S4). The increased N fixation activity does not translate to a greater growth rate in the mutant, however, suggesting possible compensatory modifications in downstream steps of N metabolism.

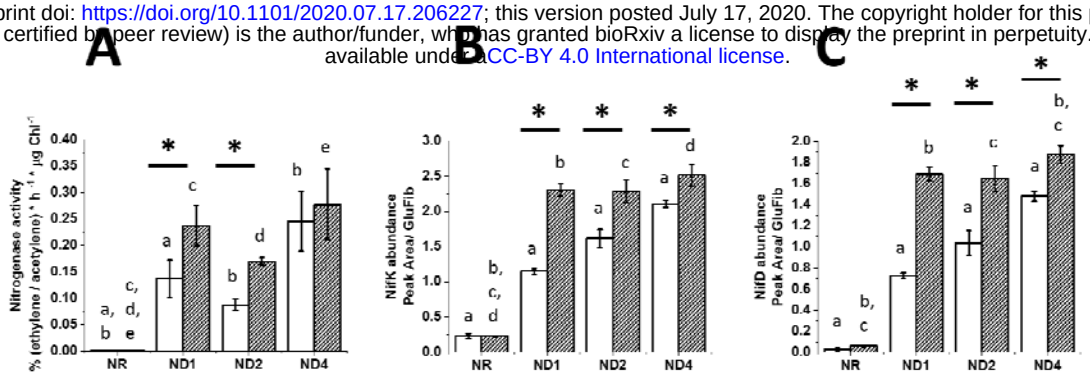

Figure 5. Nitrogenase activity (A), NifK (B) and NifD (C) abundance in both WT and Δamt strains, following N deprivation. *Time points are those indicated in Fig. 4A and correspond to NR (Nitrogen Replete), ND1, ND2 and ND4, respectively 1, 2 and 4 days after Nitrogen Deprivation. Data are indicated as average ± SD of 6 biological replicates. Statistically significant differences between WT (white bars) and Δamt (striped bars) are indicated with an asterisk, whilst the same alphabet letter indicates statistically significant differences for the same strain in different growth conditions (one-way ANOVA, p-value < 0.05).*

Once atmospheric N is fixed into ammonium/ammonia, the latter is incorporated into amino acid metabolism. GS activity was strongly regulated in both strains also in this experiment, as observed before (Fig. 2B). In N replete conditions, Δ*amt* showed greater N assimilation activity than the parental strain (i.e. NR in Fig. 6A), likely to be the cause of the increased influx of N in the central metabolism, as indicated by the increased pigment content and photosynthetic activity observed in NR conditions (Table 1 and Fig. 4B). Consequently, GS activity was influenced by the change in N metabolism, especially in the earlier samples. GS activity was at first reduced and then strongly increased (i.e. ND1 and ND2 in fig. 6A), before stabilising again to the same rate observed under N replete conditions (i.e. ND4 in fig. 6A). The trend in GS activity appeared to depend on the abundance of both GS and IF7A (Fig. 6B and 6C, respectively), which accumulate differentially in the two strains. The deletion of the whole *amt* cluster in fact strongly affects the abundance of both proteins, which impacts the overall regulation of GS activity, possibly calling for other compensatory mechanisms in this genetic background, as often GS activity is retained even though differences in the amount of IF7A are present (Fig. 6D). These results strengthen the hypothesis that AMT transporters play a direct or indirect IF7A-independent role on the GS activity in 7120.

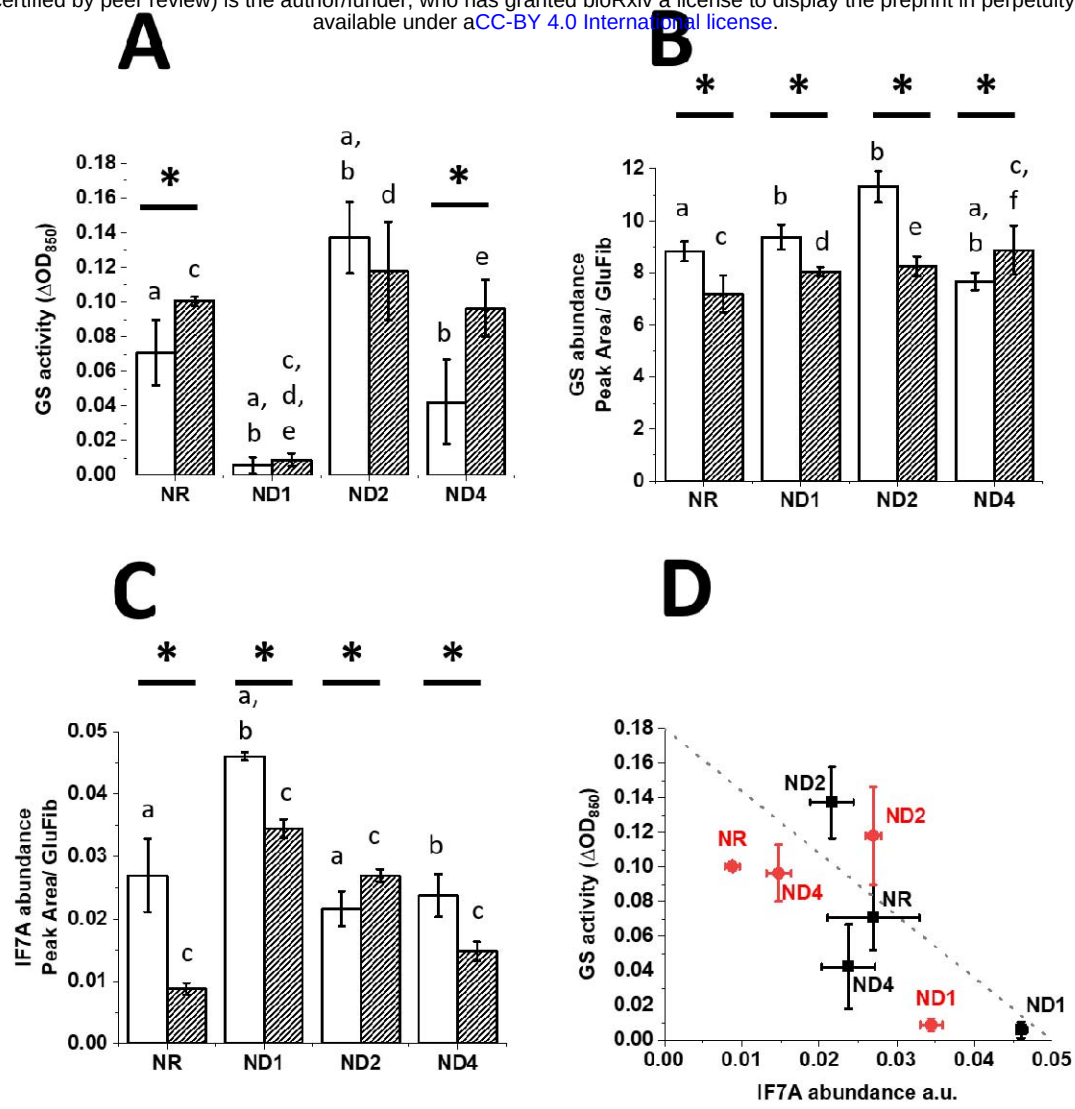

Figure 6. Regulation of N assimilation during the switch towards N deprivation in both 7120 WT and Δamt strains. *A. GS activity; B. GS abundance; C. IF7A abundance; D. Correlation between GS activity and IF7A abundance. Time points are those indicated in Fig. 4A and correspond to NR (Nitrogen Replete), ND1, ND2 and ND4, respectively 1, 2 and 4 days after Nitrogen Deprivation. Data are indicated as average ± SD of 6 biological replicates. Statistically significant differences between WT (white bars and black squares) and Δamt (striped bars and red circles) are indicated with an asterisk, whilst the same alphabet letter indicates statistically significant differences for the same strain in different growth conditions (one-way ANOVA, p-value < 0.05).*

GS is the major entry point of fixed N in the central metabolism of 7120 (Bolay *et al*, 2018). Nevertheless, other enzymes control the availability of GS substrates, thus indirectly contributing to the regulation of N assimilation. These include GOGAT (responsible for the regeneration of Glu in the GS-GOGAT cycle), IDH (responsible for the synthesis of 2-OG, a substrate of GOGAT) and GDH (involved in the reversible conversion between Glu and 2-OG) (Martín-Figueroa *et al*, 2000; Bolay *et al*, 2018; Forchhammer & Selim, 2019). Under the tested experimental conditions, the deletion of the whole *amt* cluster had major consequences also on the abundance of such enzymes (Supplementary fig. S5). GOGAT accumulation followed the same trend in both strains over the course of the experiment (i.e. strong downregulation as a consequence of N deprivation, supplementary fig. S5A), while IDH and GDH displayed different trends in the two genetic

backgrounds (Supplementary fig. S5B and S5C, respectively). These observations support the notion that the absence of AMT transporters triggers both direct and indirect effects on N metabolism in 7120.

The absence of AMT transporters affects the master regulatory network of N metabolism

Given the impact of Δ*amt* on both GS and nitrogenase, the question is how widespread the adjustments had rippled further into the cellular system? In order to address this question, we investigated the N metabolism more deeply, with an expanded number of protein quantification targets. The C/N balance of the cell is in fact also known to regulate the interaction between NctA, PipX and PII in 7120 (Forchhammer & Selim, 2019), which are expected to be the major molecular players controlling the metabolic remodelling in response to both the nature and availability of N source in the external environment, in 7120 (Fig. 1). The transcription factor NtcA, active only once bound to PipX, regulates the abundance of nitrogenase, GS and IF7A (Flores & Herrero, 2005). As Δ*amt* both responds to N deprivation more quickly than the parental strain, by activating faster N fixation (Fig. 5), and also shows major alterations in the regulation of N assimilation (greater GS activity), we wondered whether the mutation might have an effect on such master molecular regulators, which control both enzymatic steps in this species (i.e. NtcA, PII and PipX, Fig. 1) and we thus quantified their abundance (Fig. 7).

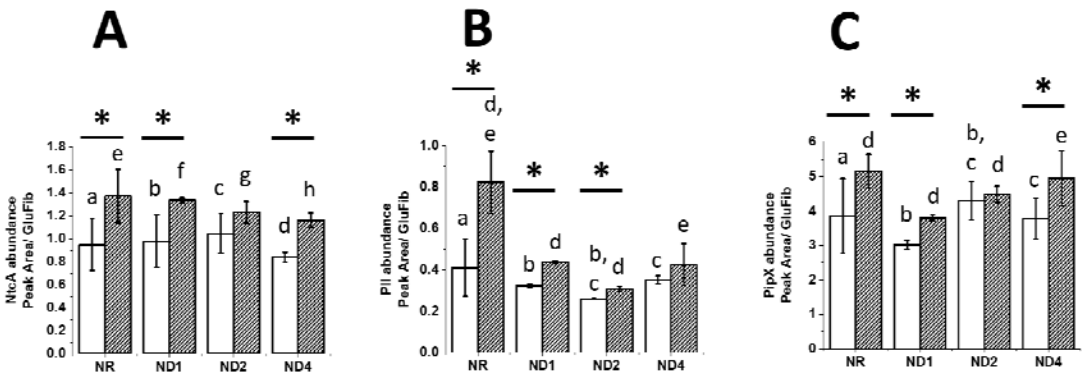

Figure 7. Abundance of the three major molecular players regulating N metabolism in 7120. *A. NtcA; B. PII; C. PipX. Time points are those indicated in Fig. 4A and correspond to NR (Nitrogen Replete), ND1, ND2 and ND4, respectively 1, 2 and 4 days after Nitrogen Deprivation. Data are indicated as average ± SD of 6 biological replicates. Statistically significant differences between WT (white bars) and Δamt (striped bars) are indicated with an asterisk, whilst the same alphabet letter indicates statistically significant differences for the same strain in different growth conditions (one-way ANOVA, p-value < 0.05).*

Overall, Δ*amt* accumulated more of the three proteins over the course of the experiment relative to the parental strain, suggesting the absence of AMT transporters has an extensive impact on the cellular system, involving the master regulatory network of N metabolism. This might explain the more rapid activation of N -fixation in response to N deprivation and also the effect on N assimilation, discussed above (Fig. 5 and Fig. 6). Moreover, while the abundance of the three proteins does not vary much over the course of the experiment in WT, PII does respond to N deprivation and is more abundant under NR conditions in Δ*amt* (Fig. 7B). This suggests PII might be

348 degraded after induction of N deprivation, possibly as a consequence of a greater phosphorylation
349 rate (see Fig. 1 for the molecular mechanisms controlling PII/PipX interaction). These results
350 strengthen the notion that AMT transporters play a central role in the regulation of N metabolism in
351 7120.
352
353 *Metabolic remodelling as a consequence of amt deletion*
354 Under diazotrophic conditions, coordinated metabolic interaction between vegetative cells and
355 heterocysts is seminal for optimal growth. The absence of AMT transporters triggered an extensive
356 remodelling at the protein level in 7120, spanning both cell types, given some of the proteins
357 investigated in this work are known to be exclusively expressed in one of the two cell types [e.g.
358 GOGAT in vegetative cells, (Martín-Figueroa *et al*, 2000)]. We therefore wondered whether the same
359 also happens at the metabolite pool level. Cyanobacteria evolved the ability to store assimilated N in
360 the form of cyanophycin granule polypeptide (CPG), possibly acting as a buffer to naturally varying N
361 -fixation due to fluctuations in N supply and day/night cycles (Watzer & Forchhammer, 2018). In
362 heterocystous filamentous cyanobacteria, CPG accumulates at the contact sites between heterocysts
363 and adjacent vegetative cells and is expected to regulate the transfer of fixed N from the former to
364 the latter (Burnat *et al*, 2014), thus influencing metabolite exchange between the two cell types (see
365 supplementary Fig. S6A for a schematic overview of CPG metabolism in 7120). In order to investigate
366 whether the metabolites exchange between the two cell types was also affected by the mutation,
367 we studied potential alterations in the CPG metabolism (Fig. 8).

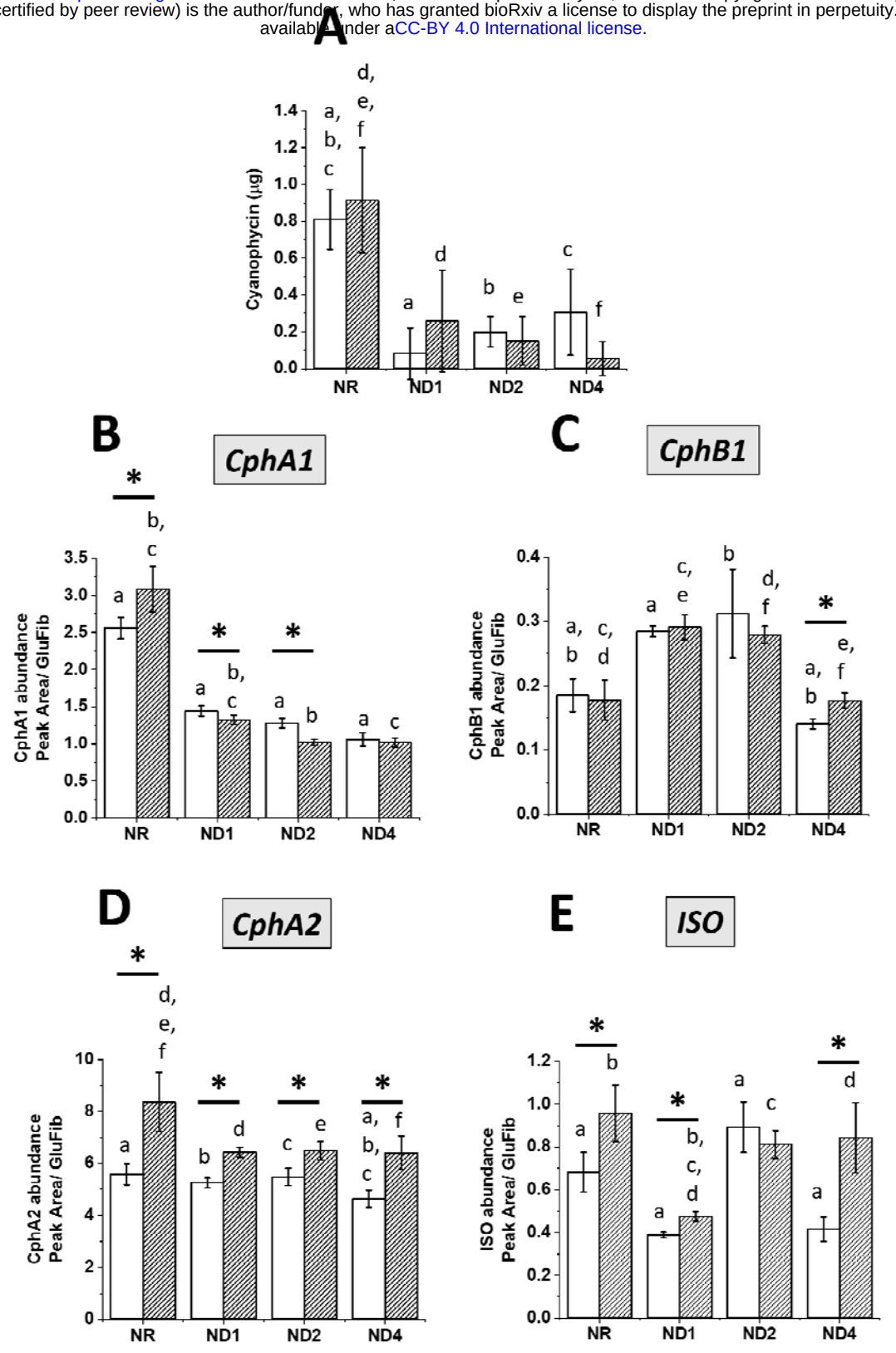

368

369 ***Figure 8. Cyanophycin (CPG) content and abundance of the four major enzymes regulating its metabolism in***
370 ***both WT and Δamt strain.*** *A. Cyanophycin content in both WT and Δamt strains in the four time points chosen*
371 *in this experiment, according to Fig. 4A. The same amount of biomass was processed in all conditions for both*
372 *strains (see materials and methods). B, C, D and E. Abundance of the four major proteins [i.e. Cyanophycin*

synthetase (CphA1), Cynaophycinase (CphB1), Cyanophycin synthetase 2 (CphA2) and Isoaspartyl dipeptidase (ISO), respectively for B, C, D and E] regulating cyanophycin metabolism in 7120, in the four time points chosen in this experiment (Fig. 4A). Data are indicated as average ± SD of 6 biological replicates. Statistically significant differences between WT (white bars) and Δamt (striped bars) are indicated with an asterisk, whilst the same alphabet letter indicates statistically significant differences for the same strain in different growth conditions (one-way ANOVA, p-value < 0.05). See supplementary fig. S6 for an overview of CPG metabolism.

Under the tested experimental conditions, both strains accumulated CPG in NR conditions as expected (Forchhammer & Watzer, 2016), suggesting the deletion of AMT transporters did not perturb N storage to the point of affecting CPG accumulation. In fact, both strains show the same CPG content in NR (Fig. 8A), indicating the pool of available CPG to support the metabolic needs of the cell is not affected by the mutation at this time point. Nevertheless, the abundance of three out of four major enzymes controlling CPG metabolism (Supplementary Fig. S6) is significantly different between the two strains, with CphA1, CphA2 and ISO showing increased accumulation in the mutant with respect to the parental strain in NR (Fig. 8B, D and E). We therefore hypothesised that the overall CGP metabolic flux is accelerated in the mutant under NR conditions, possibly enabling a faster response to environmental changes. When cells experience N deprivation, the cyanophycin content decreases, presumably as it is rapidly used as N source (Forchhammer & Watzer, 2016) (i.e. after one day of N deprivation CPG is fully consumed, Fig. 8A). Nevertheless, whilst CPG starts building up again in the parental strain after two days of N deprivation, a constant consumption trend is observed over the course of the experiment in the mutant (Fig. 8A). This suggests that N fixation in the WT exceeds metabolic needs and a fraction of the assimilated N is thus stored as CPG, while in the mutant this trend is disrupted. Out of the four major enzymatic steps controlling CPG metabolism in 7120, cyanophycin synthetase (CphA1), the major enzyme controlling CPG biosynthesis (Forchhammer & Watzer, 2016), is most affected by N deprivation (Fig. 8 B, C, D and E), with the mutant showing a faster reduction in its abundance than the parental strain (Fig. 8B). It is also worth noting that cyanophycin synthetase 2 (CphA2), a truncated version of CphA1 catalysing the direct recycling of the β-aspartyl-arginine dipeptide into CPG (Supplementary Fig. S6, (Forchhammer & Watzer, 2016)], is more abundant in the mutant strain in all time points (Fig. 8D), strengthening the notion that CPG metabolism is accelerated in Δ*amt*.

CPG accumulation in N fixing cyanobacteria is mediated by PII which in turn regulates N-acetyl-N-glutamate kinase (NAGK) activity (Forchhammer & Selim, 2019). NAGK catalyses the conversion of N-acetyl-L-glutamate to N-acetyl-L-glutamyl-phosphate, which is further converted to ornithine, from where Arg, the end -product of the pathway, is derived. Therefore, CPG biosynthesis directly follows the concentration of free Arg in the cell, as a consequence of feedback inhibition of NAGK (Watzer *et al*, 2015). In our experimental conditions, the free Arg concentration indeed strongly decreased upon N deprivation in both strains (Fig. 9A and B), confirming the strong reduction in CPG content upon N deprivation, observed before (Fig. 8A).

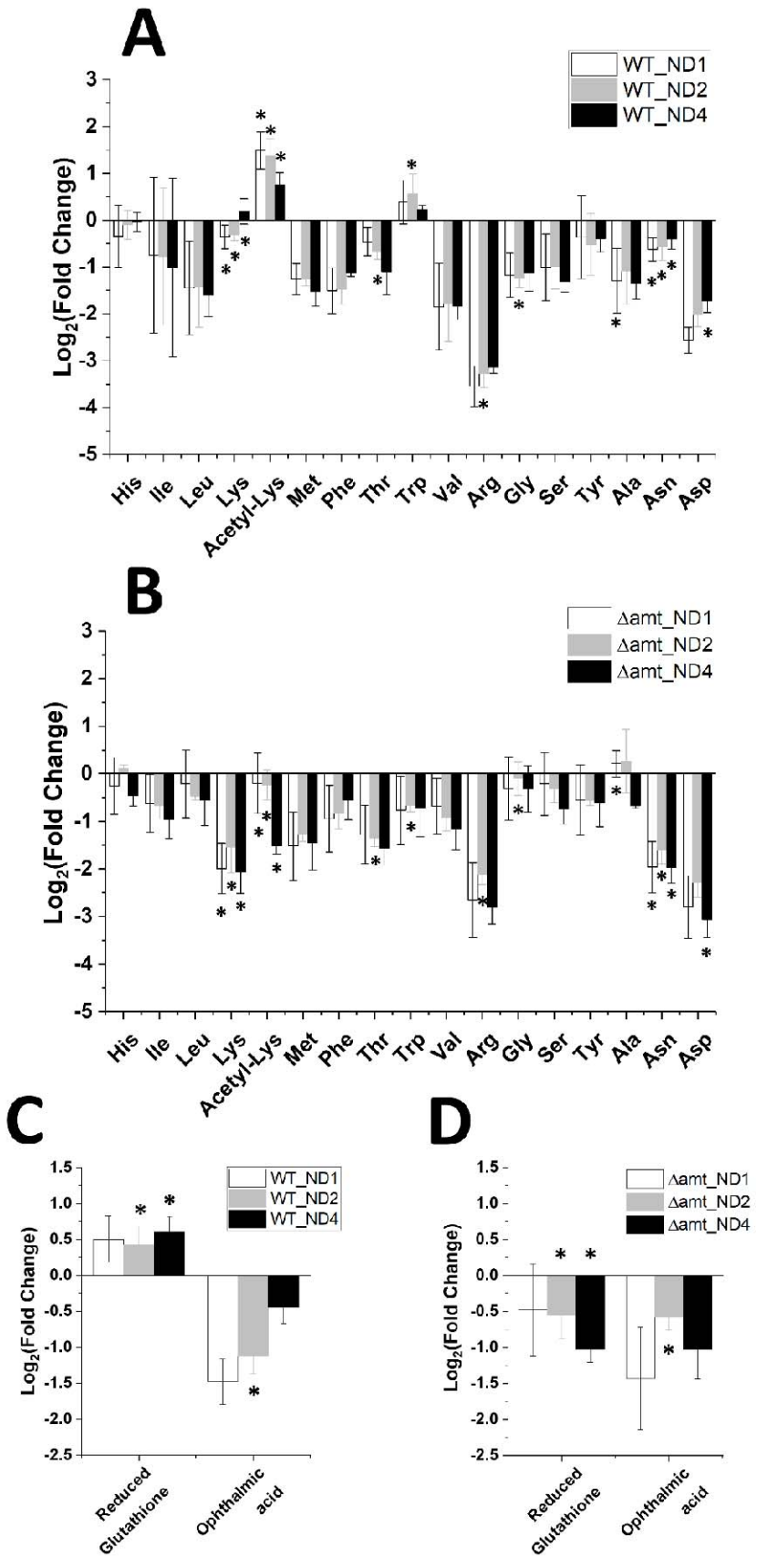

Figure 9. Pool of free amino acids and oxidative stress markers in both WT and Δamt strain, upon N deprivation. *Free amino acid pool (A and B) and oxidative markers (C and D) in the WT strain (A and C) and in the Δamt mutant (B and D) in the four time points chosen in this experiment, according to Fig 4A. Data are expressed as base two logarithm of the fold change (FC) of the abundance of each metabolite between each of the three time points after N deprivation (i.e. ND1, 2 and 4) and N replete conditions (NR). Data are indicated as average ± SD of 6 biological replicates. Statistically significant differences between WT and Δamt for each metabolite at a specific time point are indicated with an asterisk (one-way ANOVA, p-value < 0.05).*

Overall, both strains display a reduction in the whole pool of free amino acids as a consequence of N deprivation (Fig. 9A and B), likely suggesting a faster turnover upon N-fixing conditions. Nevertheless, upon N deprivation, the Δ*amt* strain also shows substantial remodelling of the free amino acid pools (Fig. 9B), relative to the parental strain (Fig. 9A). Major amino acids affected by the mutation are Lys and Asn, which display a stronger reduction in the mutant upon N deprivation, followed by Thr, Trp, Arg, Gly, Ala and Asp (Fig. 9B), which instead show minor but still relevant alterations. These results indicate a comprehensive impact on the amino acid metabolism in 7120 as a consequence of the mutation. It is also worth noting the pool of acetyl-lysine is differentially regulated in the two strains upon N deprivation (Fig. 9A and B), suggesting a comprehensively different regulation of the whole central metabolism.

Amino acids are substrates for the synthesis of several molecular players, important for the homeostatic control of the cell. Among them, glutathione (Cameron & Pakrasi, 2010) and ophthalmic acid (Ito *et al*, 2018) belong to a robust antioxidant buffering system which plays an important role in protecting against reactive oxygen species (ROS) generated as by-product of photosynthetic metabolism (Narainsamy *et al*, 2016).

Interestingly, while no major differences between the two strains were observed for ophthalmic acid upon N deprivation, the content of reduced glutathione (GSH) increased in WT (Fig. 9C) and it decreased in Δ*amt* (Fig. 9D), suggesting the mutant suffers from redox stress upon N deprivation.

Gln, Glu and 2-OG pools

The metabolic pool concentration of several key metabolites in N metabolism, Gln, Glu and 2-OG [Fig. 1, (Martín-Figueroa *et al*, 2000; Böhme, 1998; Picossi *et al*, 2005)], was also affected by the *amt* mutation. The pool of free Glu increased in both strains over the course of the experiment (Fig. 10A and B), whilst the concentration of Gln dropped substantially in the wild-type upon N deprivation (Fig. 10A). Interestingly, the concentration of Gln is several-fold lower in Δ*amt* under N replete conditions and also drops upon elimination of assimilable N (Fig. 10B). Hence, the Gln/Glu ratio in the mutant is indicative of a partially deprived N metabolic state even in the presence of assimilable N (Supplementary Fig. S7), potentially affecting also the metabolic exchange between the two cell types (no difference in the number of heterocysts was observed between the two strains over the course of the experiment, see Supplementary Fig. S4). Similarly, the mutant also has a slightly lower 2-OG content than the parental strain under NR conditions (Fig. 10C), and consequently a higher 2-OG/Gln ratio (Supplementary Fig. S8), in line with the hypothesis that 2-OG is indicative of metabolic N availability (Muro-Pastor *et al*, 2001). The difference between the two strains is admittedly small, at only around 18% – but then, the decrease in 2OG following N deprivation is only about 40%, so even this small decrease could represent a change in N status.

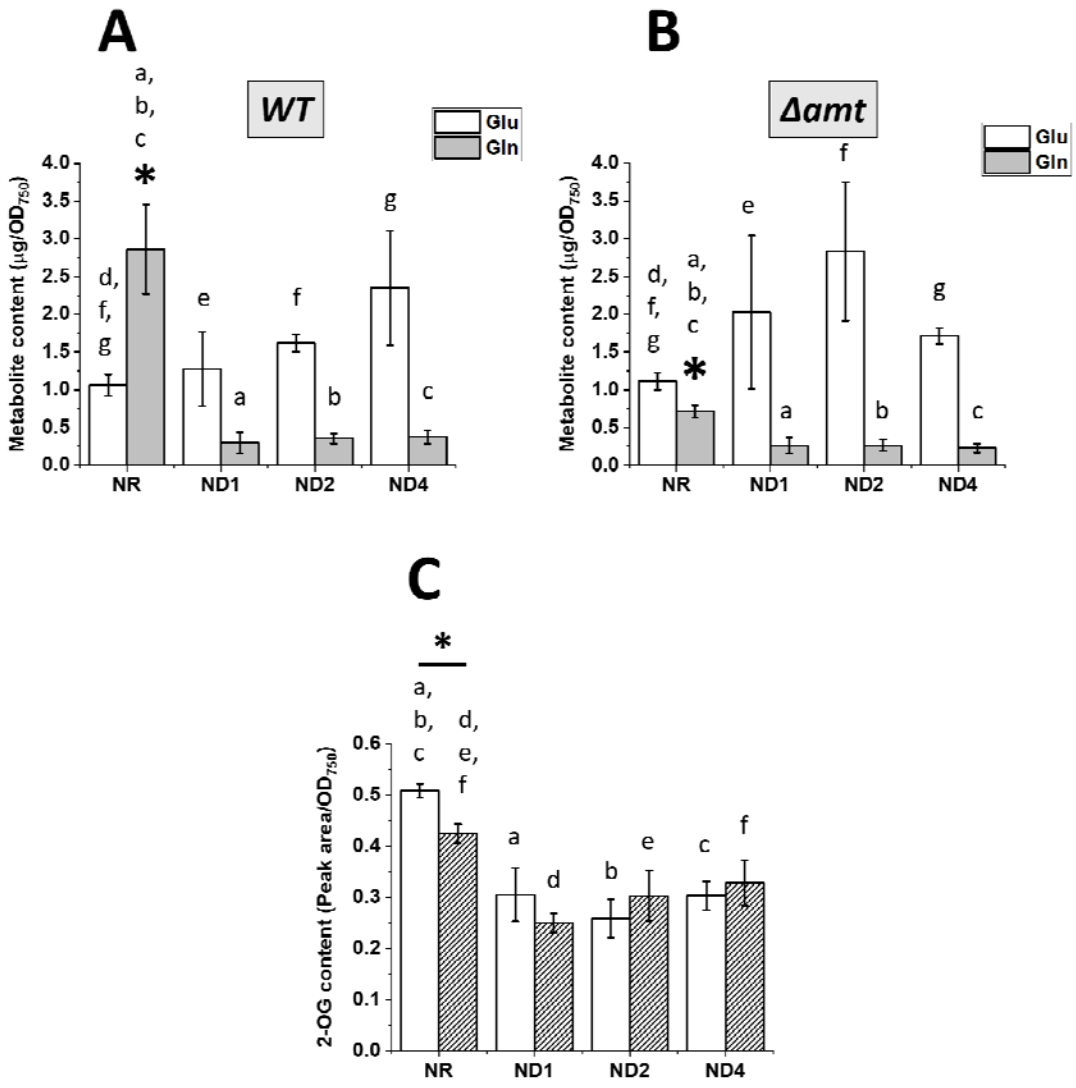

460 ***Figure 10. Metabolic pool concentration of key metabolites in N metabolism.*** *Glu, Gln (A, B) and 2-*
461 *OG (C) content in 7120 WT and Δamt strains, in the experimental conditions of Fig. 4A. Glu (white*
462 *bars) and Gln (grey bars) content is split in two distinct panels for WT (A) and Δamt (B). C. 2-OG*
463 *content in WT (white bars) and Δamt (striped bars). Results come from the same amount of biomass*
464 *for both strains and for different growth conditions. Data are indicated as average ± SD of 6*
465 *biological replicates. Statistically significant differences between WT and Δamt for each metabolite*
466 *at a specific time point are indicated with an asterisk, whilst the same alphabet letter indicates*
467 *statistically significant differences for the same strain and metabolite, in different growth conditions*
468 *(one-way ANOVA, p-value < 0.05).*
469
470

Discussion

Biological systems can be fuelled by multiple N sources, but they are all converted to ammonium/ammonia before assimilation, as the latter is the most reduced and energetically favourable bioavailable form of N. The translocation of ammonium/ammonia across biological membranes is therefore expected to play a potential key role in the regulation of N metabolism. Active ammonium/ammonia translocation [whether it involves the charged or uncharged form is still debated and it is likely to depend on the species in question (Ludewig, 2006; Ludewig *et al*, 2007; Boogerd *et al*, 2011; Wang *et al*, 2012; Javelle *et al*, 2007)] across biological membranes is catalysed by AMT transporters, a protein family widely distributed across multiple domains of life (Andrade & Einsle, 2007).

In this work we exploited a KO mutant of the whole *amt* cluster (i.e. *Δamt*) in *Anabaena sp. PCC 7120* (Paz-Yepes *et al*, 2008) to perturb both sensing and uptake of $NH4^+$, with the aim to investigate how a N_2-fixing cyanobacterium responds to perturbation of N -metabolism at a whole cell level.

We cultivated both 7120 WT and *Δamt* strains in different N regimes (i.e. different N sources and N replete/deplete conditions). The underlying idea was to trigger different inner N states and investigate them through physiological, proteomic and metabolomic analyses. Upon N deprivation, *Anabaena sp. PCC 7120* differentiates a fraction of its cells into heterocysts to enable efficient N fixation (Golden & Yoon, 1998; Kumar *et al*, 2010), posing several limitations to integrated studies such as this one. One of them is the need to process the samples as a mixture of the two cell types, in order to avoid metabolic changes that are inevitable consequence of physical separation (Ermakova *et al*, 2014). This necessary choice forgoes discrimination of the metabolic status of the two cell types. Nevertheless, some proteins and metabolites are unique to one of the two cell types (Martín-Figueroa *et al*, 2000), enabling to partially overcome such limitations. Moreover, we did not observe any difference in the ratio of heterocysts to vegetative cells in response to any of the genetic or environmental treatments investigated in this work (Supplementary Fig. S4).

Lack of AMT transporters triggers a substantial response at the whole cell level, but doesn't induce any visible phenotype

In the constant laboratory conditions tested in this work, we observed AMT transporters are not essential to support growth of 7120, regardless of the N source used to sustain the central metabolism (Fig. 2A and 4A), as previously reported (Paz-Yepes *et al*, 2008). This finding corroborates what has been observed in other bacteria [e.g. *Rhodobacter capsulatus* (Yakunin & Hallenbeck, 2002)], suggesting a conserved transporter-independent function for AMT transporters across unrelated bacteria species.

Nevertheless, the mutant surprisingly displays several changes in the abundance of proteins and metabolite pools with a central role in N metabolism, triggering also a substantial effect on key enzymatic activities. Among them, we observed: (1) a substantial increase in nitrogenase activity (Fig. 2B and 5A), likely due to an increased accumulation of the protein complex (Figure 5B and 5C); (2) an increased GS activity in $NH4^+$-replete conditions and upon prolonged N deprivation (Fig. 2C and 6A), as a consequence of changes in the abundance of proteins which play both a direct and/or indirect role on GS activity such as: (a) changes in the abundance of both the GS protein itself (Fig. 3A and 6B) and the post-translational negative regulator IF7A (Supplementary Fig. S3 and Fig. 6C) and (b) changes in the abundance of GDH, GOGAT and IDH, which re-generate its substrates (Supplementary Fig. S5). It is worth noting that some of these observations correlate with what has already been observed in other organisms, such as the photosynthetic purple bacterium *Rhodobacter capsulatus*, in which the absence of the AMTB transporter influenced both nitrogenase

and GS activity, thus strengthening the hypothesis that such proteins might share the same role in the regulation of N metabolism, even in distinct bacteria species (Yakunin & Hallenbeck, 2002). Moreover, we also observed that the pool of free amino acids (Fig. 9A and 9B), redox markers (Fig. 9C and 9D) and metabolites with a key role in N metabolism orchestration (i.e. Gln, Glu and 2-OG, Fig. 10) is affected by the mutation. The *Δamt* mutant also displays substantial changes in photosynthetic performances and pigment content with respect to the parental strain (Fig. 4B and Table 1).

It is worth noting that the biochemical changes observed in the mutant do not translate in any phenotypic difference with respect to the parental strain (i.e. growth is unaffected, Fig. 2A and Fig. 4A), highlighting the strong robustness of the biological system under investigation. The latter most likely depends on its ability to undergo this very substantial homeostatic adjustment at the whole cell level, as a consequence of both genetic (i.e. *Δamt*) and environmental treatments (i.e. different N regimes).

Lack of AMT transporters induces metabolic adaptation spanning both C and N metabolism, with a potential impact on the metabolites exchange between heterocysts and vegetative cells

As in many biological systems, N and C metabolism is expected to be tightly coupled (Zhang *et al*, 2018) also in 7120, thereby maintaining a properly balanced C/N ratio even when exposed to external perturbations (Forchhammer & Selim, 2019). When the C source (i.e. CO_2 in case of phototrophic metabolism) is not limiting, external N source(s) are expected to directly influence the C/N balance of the cell, with both: (1) efficiency in sensing and uptake and (2) abundance and nature of such N source(s) playing a central role. In our experiments, 7120 was cultivated in a 1% CO_2-enriched atmosphere in order to avoid C limitation and both genetic (i.e. *Δamt* mutation) and environmental (i.e. different N sources and abundance) treatments were used to perturb both such parameters and investigate the response of 7120 at a whole cell level.

The mutant displayed substantial changes in the abundance of several metabolites (Fig. 9), including Gln, Glu and 2-OG. Among them, it is worth noting the difference in the free pool of acetyl-lysine (Fig. 9A and 9B) which suggests the overall central metabolism regulation might be comprehensively affected as a consequence of the mutation (Nakayasu *et al*, 2017; Christensen *et al*, 2019). The observed differences in the free pool of acetyl-lysine might reflect either changes in total protein acetylation, or else changes in the turnover rates of acetylated proteins, with a potential regulatory role in both photosynthesis and carbon metabolism, as suggested in *Synechocystis sp. PCC 6803* (Mo *et al*, 2015). Further confirmation in the lab is however needed to clarify the regulatory role of protein acetylation in 7120.

Differences in the accumulation of Gln, Glu and 2-OG are a clear hallmark of a perturbed C/N balance (Fig. 10). Gln, Glu and 2-OG are in fact key metabolites involved in the GS-GOGAT cycle, hence they play a critical role in the central crossroad for C and N metabolism. Moreover, Gln and Glu metabolism is intertwined with that of several other amino acids as they are the most important amino groups donor for their synthesis (Reitzer, 2003; Huergo & Dixon, 2015), whilst 2-OG is the major signalling metabolite used to perceived the intracellular N status by cyanobacteria (Muro-Pastor *et al*, 2001). In our experiments, 2-OG concentration decreased upon N deprivation (Fig. 10C) and this correlates with the observed increase in the pool of free Glu (Fig. 10A and 10B), as cyanobacteria lack 2-OG dehydrogenases and therefore 2-OG is mainly used for the biosynthesis of Glu or other Glu-derived compounds (Herrero *et al*, 2001). It is worth noting that this trend is not affected by the mutation (Fig. 10C), which instead induces a reduction in the content of 2-OG in NH_4^+-replete conditions (Fig. 10C).

Taken together, these data suggest the absence of AMT transporters results in a metabolic adjustment in response to environmental treatments (i.e. different N regimes), and although not investigated in the present study, this is likely to affect also the traffic of metabolites between heterocysts and vegetative cells, as also suggested by the observed differences in CPG metabolism (Fig. 8).

Are AMT transporters an integral part of the N metabolism regulatory/signalling network?

In our experiments, we repeatedly observed substantial changes in GS activity as a consequence of the mutation. The mutant in fact displays an increased GS activity in NH_4^+ replete and also in prolonged N deplete conditions (Fig. 6A and Fig. 2C), likely in response to changes in the abundance of both the GS protein itself and its post-translational regulator IF7A (Fig. 3 and 6). Moreover, we observed that GS activity is often retained even if IF7A abundance varies, potentially suggesting an additional molecular player(s) might also be involved in its regulation. Taken together, our results suggest AMT transporters might play a direct or indirect IF7A-independent role on GS activity in 7120, thus calling for further scientific efforts in order to fill potential gaps in the regulatory/signalling network of N metabolism.

The changes observed in this work are widespread at a whole cell level, also affecting the master molecular players which orchestrate N metabolism (i.e. NtcA, PII and PipX, Fig. 7). In particular, the mutant displays an increased PII abundance in NR conditions, with respect to the parental strain (Fig. 7B). PII belongs to one of the most widely distributed families of signal transduction proteins in nature, involved in various aspects of N metabolism and regulation of C/N homeostasis (Forchhammer, 2004, 2008; Arcondeguy *et al*, 2001; Forcada-Nadal *et al*, 2018). Among them, in heterotrophic bacteria and in archaea, PII proteins of the subfamily GlnK directly interact with AMT transporters to regulate their activity, typically reducing their uptake rate in N excess conditions to prevent intracellular over-accumulation of ammonium (Arcondeguy *et al*, 2001). Recent studies suggest PII protein binds AMT transporters also in cyanobacteria [i.e. *Synechococcus sp. PCC 7942* (Forchhammer & De Marsac, 1995) and *Synechocystis sp. PCC 6803* (Watzer *et al*, 2019)]. Our observation of a greater PII abundance, as a consequence of a deletion in AMT transporters, supports the hypothesis that PII might retain this function also in 7120. If true, this suggests one potential mechanism for how AMT transporters might influence the regulatory/signalling network of N metabolism in 7120.

It is worth noting that the molecular fingerprint of *Δamt* cells display symptoms of N -deficiency relative to the parental strain, also in NH_4^+ replete conditions, and that observations at both protein and metabolite level support this hypothesis. Among them: (1) the faster activation of nitrogenase upon N deprivation (Fig. 5A), (2) the increased GS activity (Fig. 6A), (3) the strong reduction in the Gln/Glu ratio (Supplementary Fig S7), (4) the slightly reduced 2-OG content (Fig. 10C) and (5) the increased 2-OG/Gln ratio (Supplementary Fig. S8). In contrast, the greater photosynthetic activity (Fig. 4B) and Chl/Car ratio (Table 1) suggest the mutant does not suffer from N limitation in NR conditions. This raises the interesting question: what is cause and what is effect? The observed changes at the protein level are coupled to a widespread metabolic adaptation as a consequence of the mutation, involving substrates and products of most of the enzymatic reactions investigated at the protein level. In fact, it is reasonable to expect that some of the changes in the accumulation of specific proteins might simply result from an adaptation to perturbations of the metabolite pool or *vice versa*. At this point, we thus cannot conclude whether the *Δamt* mutant either is directly suffering from an imbalanced regulatory/signalling network or if it suffers from perturbations at the metabolite level, which are sensed by such regulatory/signalling network.

609 However, AMT transporters play a direct or indirect role in the regulatory/signalling network which
610 still warrant further investigations.
611

Conclusions

We investigated how a mutant of *Anabaena sp. PCC 7120*, impaired in both sensing and low-affinity up-take of NH_4^+, responds to environmental treatments affecting the inner N status of the cells. The whole cell system responds with substantial internal perturbations embracing both N and C metabolism. Moreover, the absence of AMT transporters leaves a molecular fingerprint suggesting N-deficiency, which surprisingly does not lead to any externally measurable phenotypic effects. We thus hypothesise that 7120 evolved a robust regulatory/signalling molecular network to maintain N metabolism homeostasis. The observed changes involve both proteins and metabolites, highlighting a pleiotropic effect of the mutation. We also provided evidence of perturbations to nitrogenase and GS activity, as well as to master regulators orchestrating N metabolism, thus leading to the hypothesis that a possible direct or indirect IF7A-independent role of AMT transporters on GS activity exists in 7120, possibly transduced via the PII protein. Taken together, these evidences suggest AMT transporters might play an active role in the regulatory/signalling network, calling for further scientific efforts in order to fill current gaps in N metabolism homeostasis. The work highlights the dynamic and complex nature of internal mechanisms involved in maintaining homeostasis and the success in so doing, achieving a near-complete lack of any measurable external impact.

Material and Methods

Cyanobacteria strains and growth conditions

Strains of *Anabaena sp. PCC 7120* used in this work are summarised in table 2 and were kindly provided by Prof. Enrique Flores [institute of Plant Biochemistry and Photosynthesis, University of Sevilla (Sevilla, Spain)].

Table 2. Strains of Anabaena sp. PCC 7120 used in this work.

Strain	Genotype	Source
***Anabaena sp. PCC 7120* WT**	Wild-type (WT)	Prof. Enrique Flores
Anabaena sp. PCC 7120 Δamt	Δamt::C.K3; Amt4$^-$, Amt1$^-$, AmtB$^-$, Nm^R	(Paz-Yepes *et al*, 2008)

Both strains were maintained in solid BG11 medium (pH 8.0 with the addition of 10 mM final concentration of TES-NaOH buffer) (Rippka *et al*, 1979) (1.5% Difco Bacto agar, BD) in an Algaetron 230 (PSI, Photon Systems Instruments, Czech Republic), with an atmosphere enriched in CO_2 (1%), under cool white light at 60 µmoles of photons*m^{-2}*s^{-1}, 30 °C. Illumination rate was determined using a LI-250A photometer (Heinz-Walz, Effeltrich, Germany). Before starting an experiment, both strains were switched to liquid medium and pre-cultivated axenically in 100-ml Erlenmeyer flasks in 20 ml $BG11_0$ (BG11 medium, without $NaNO_3$) supplemented with 5 mM NH_4Cl in the same growth conditions, under orbital shaking at 160 rpm. Cells were kept in exponential growth conditions, refreshing the cultures every other day (i.e. replacing half of the volume of the culture with fresh $BG11_0$ + 5 mM NH_4Cl). *Anabaena sp. PCC 7120* Δamt strain was cultivated in presence of 10 µg/ml neomycin (Nm).

For all experiments carried out in this work, strains were cultivated in 6-well polystyrene plates in the same growth conditions indicated above. Cells pre-cultivated in Erlenmeyer flasks were washed twice in the final growth medium, through centrifugation for 10 min, 3500 g, RT. Starting OD_{750} for all growth curves = 0.1. Media at different pH values were obtained using 10 mM final concentration of phosphate, TES-NaOH and CAPS buffers, respectively for pH 6.0, 8.0 and 10.0.

Growth was monitored through OD_{750} in 96-wells polystyrene plates with a multimode spectrophotometer (Tecan Infinite M200 Pro). Linear correlation between OD_{750} and biomass dry weight was confirmed for both strains and the growth ranges measured in this work. Biomass dry weight was measured gravimetrically as previously reported in (Perin *et al*, 2015). Specific growth rate was calculated by the slope of different growth phases for growth curves plotted in logarithmic scale.

Pigments content and photosynthetic efficiency

Pigments from intact cells grown in 6-wells plates were extracted using a 1:1 biomass to solvent ratio of 100% methanol, at 4 °C in the dark for at least 20 min (Sinetova *et al*, 2012). Absorbance at 470, 665 and 730 nm was monitored using a multimode spectrophotometer (Tecan Infinite M200 Pro) to determine pigment concentrations, using specific extinction coefficients (Ritchie, 2006; Wellburn, 1994).

Photosynthetic efficiency was assessed measuring *in vivo* chlorophyll fluorescence of intact cells using an AquaPen-C AP 110-C (PSI, Photon Systems Instruments, Czech Republic). Photosystem II (PSII) functionality was assessed as PSII maximum quantum yield (Φ_{PSII}), according to (Maxwell & Johnson, 2000).

673 **Ammonium/ammonia quantification**

674 Ammonium/ammonia quantification was performed using an adaptation of the method described
675 by Willis et al. (Willis *et al*, 1996) in order to enable the use of 96-well microtiter plates. Briefly,
676 *Anabaena sp. PCC 7120* strains grown in 6-well plates were harvested by centrifugation and 10 µl of
677 the cell-free supernatant were loaded in a flat-bottom 96-well plate. 200 µl of reactive solution (32
678 g/L sodium salicylate, 40 g/L $Na_3PO_4 \cdot 12H_2O$ and 0.5 g/L sodium nitroprusside) and 50 µl of
679 hypochlorite solution (0.25-0.37% active chlorine) were added in this order to the cell-free sample
680 and the solution made homogenous, before measuring the absorbance at 685 nm in a multimode
681 spectrophotometer (Tecan Infinite M200 Pro), after incubation for 15 min, 900 rpm, RT in a shaker
682 (PHMP, Grant Instruments). Ammonium/ammonia concentration in the cell-free samples was
683 calculated using the linear range of a standard curve prepared with serial dilutions of a NH_4Cl
684 solution.
685
686 **Enzymatic activities**

687 **Glutamine synthetase.** Glutamine synthetase (GS) activity was assessed through the method
688 detailed below, which comes from the combination of different protocols from (Bressler & Ahmed,
689 1984; Orrs *et al*, 1981; Merida *et al*, 1991).

690 *Preparation of cell-free total proteins extracts.* Strains of *Anabaena sp. PCC 7120* grown in 6-wells
691 plates were harvested by centrifugation and the supernatant discarded. Cell pellets were transferred
692 to 2 ml polypropylene tubes and disrupted twice using a TissueLyser II (Qiagen), adding the same
693 volume of acid-washed glass beads (Sigma-Aldrich) and solubilisation buffer (50 mM Hepes, 0.2 mM
694 EDTA, pH 7.3), for 5 min at 30 Hz. Tube holders were pre-cooled at -20 °C. Cell extracts were
695 collected through centrifugation for 10 s, 9000 g, 4 °C. Cell extracts were centrifuged twice for 10
696 min, 21000 g, 4 °C to eliminate cell debris and insoluble proteins. Total proteins concentration in the
697 cell-free lysate was assessed through DC protein assay (BIO RAD), following the manufacturer's
698 manual, using 96-wells plates against a BSA (bovine serum albumin) standard curve.

699 *GS activity assay.* GS catalyses the condensation of glutamate and ammonia to generate glutamine,
700 hydrolysing ATP (reaction below).

$$Glutamate + NH_3 + ATP \rightarrow Glutamine + ADP + P$$

701 GS activity can be measured indirectly, quantifying the amount of phosphate released by the
702 reaction through colorimetric assay.

703 Enzymatic assay was performed in 550 µl in 24-wells flat bottom polystyrene plates, with 50 µg total
704 proteins in 364 mM imidazole-HCl, pH 7.0, 1.82 mM NH_4Cl, 5.45 mM Na-ATP$\cdot H_2O$, pH 7.0 (prepared
705 fresh on ice), 0.52 M $MgCl_2 \cdot 6H_2O$, 91 mM sodium glutamate, pH 7.0, for 15 min, 400 rpm, 30 °C in a
706 thermoshaker (PHMP, Grant Instruments). The reaction was then quenched on ice, adding
707 $FeSO_4 \cdot 6H_2O$ (0.61% w/v in 0.011 N H_2SO_4 final concentration). In order to develop colour
708 (proportional to the amount of phosphate released by ATP as a consequence of GS activity),
709 ammonium heptamolybdate (0.4% w/v in 0.45 M H_2SO_4 final concentration) was added to the
710 reaction and solutions were homogenised on ice. Colour intensity of clear samples was measured at
711 850 nm, using a multimode spectrophotometer (Tecan Infinite M200 Pro). GS activity was calculated
712 subtracting to each sample the OD_{850} of the corresponding blank solution (prepared replacing the
713 substrate sodium glutamate with water and corresponding to the background signal of phosphate
714 released by other endogenous ATP-dependent enzymatic reactions).

715 **Nitrogenase.** Nitrogenase activity was determined with an acetylene reduction assay under oxic
716 culture conditions. Cells grown in 6-well plates were incubated in 2-ml gas chromatography glass
717 vials under an atmosphere of 10% acetylene in air. Vials were incubated for 3 h in the same original

718 growth conditions (i.e. shaking, light, 30 °C) and the quantity of ethylene in the headspace was
719 determined by gas chromatography (7820A GC system, Agilent Technologies). The nitrogenase
720 activity is expressed as % conversion of added acetylene into ethylene, per hour and per µg of Chl.
721
722 **Cyanophycin content**
723 **Cyanophycin extraction.** The same amount of biomass (OD_{750} = 0.3) of different *Anabaena sp. PCC*
724 *7120* strains grown in 6-wells plates was harvested by centrifugation and the supernatant discarded.
725 Cyanophycin was extracted from the cell pellets following the protocol detailed in (Watzer *et al*,
726 2015), with some modifications as follows. Briefly, cell pellet was resuspended in 1 ml 100% acetone
727 and incubated in a shaker for 30 min, 1400 rpm, RT. Lysed cells were then centrifuged for 17 min,
728 21000 g, RT and the supernatant discarded. Pellet was resuspended in 1.5 ml of 0.1 M HCl and
729 incubated for 1 h, 1400 rpm, 60 °C to solubilise cyanophycin polymers. Solubilised cyanophycin was
730 centrifuged for 17 min, 21000 g, RT to remove immiscible debris. Tris-HCl, pH 8.0 was added to the
731 supernatant (0.2 M final concentration) and samples incubated for 40 min, 4 °C. Samples were then
732 centrifuged for 17 min, 21000 g, 4 °C and pelleted cyanophycin polymers were resuspended in 500 µl
733 0.01 M HCl for quantification.
734 **Cyanophycin quantification.** Cyanophycin is a polymer of arginine and aspartate (Forchhammer &
735 Watzer, 2016) and the quantification of arginine released by cyanophycin granules can be used as
736 proxy for cyanophycin content determination (Burnat *et al*, 2014). Arginine quantification was
737 performed through a modified colorimetric Sakaguchi method, according to (Messineo, 1966).
738
739 **Proteomic analysis**
740 **Sample preparation.** Strains of *Anabaena sp. PCC 7120* grown in 6-wells plates were harvested by
741 centrifugation and the supernatant discarded. Cell pellets were transferred to 2 ml polypropylene
742 tubes and disrupted using a TissueLyser II (Qiagen), adding the same volume of acid-washed glass
743 beads (Sigma-Aldrich) and extraction buffer (20 mM Tris-HCl, pH 8.0, 1 mM EDTA, pH 8.0 and 2 mM
744 DTT), for 5 min at 30 Hz. Tube holders were pre-cooled at -20 °C. Cells disruption was repeated twice
745 and cell extracts were collected through centrifugation for 10 s, 9000 g, 4 °C and pulled together
746 after both cycles. Cell extracts were centrifuged twice for 10 min, 21000 g, 4 °C to eliminate cell
747 debris and insoluble proteins. Total proteins concentration was assessed through DC protein assay
748 (BIO RAD), following the manufacturer's manual, using 96-wells plates against a BSA (bovine serum
749 albumin) standard curve. Cell extracts were diluted by 0.1 M ammonium bicarbonate to have a 0.3
750 µg/µl total proteins final concentration and the standard peptide [Glu1]-Fibrinopeptide B, human
751 (GluFib, Sigma Aldrich) was added (0.3 ng/µl, final concentration). Samples were reduced by DTT and
752 ammonium bicarbonate (final concentration 10 mM and 50 mM, respectively) for 1 h, 56 °C, and
753 subsequently alkylated adding iodoacetamide prepared fresh in 0.1 M ammonium bicarbonate (50
754 mM final concentration), for 30 min, 37 °C, 500 rpm in a thermoshaker (PHMT; Grant Instruments).
755 Alkylated samples were digested by proteomics-grade trypsin (Promega), final concentration 6 ng/µl,
756 ON, 37 °C. Tryptic digestion was stopped quenching the reaction with formic acid (final
757 concentration 1%) for 30 min, 37 °C, 500 rpm in a thermoshaker. Acidified samples were centrifuged
758 at 17000 g, RT, to pellet water immiscible degradation products and the supernatant collected for
759 mass spectrometry analysis.
760 **Mass spectrometry.** Trypsin digested samples were analysed on an AB-SCIEX 6500QTrap MS coupled
761 to an Agilent 1100 LC system. Chromatography was performed on a Phenomenex Luna C18(2)
762 column (100 mm x 2 mm x 3 µm) at 50 °C, using a gradient system of solvents A (94.9% H_2O, 5%
763 CH_3CN and 0.1% formic acid) and B (94.9% CH_3CN, 5% H_2O and 0.1% formic acid). A gradient from 0

to 35% B over 30 min at a flow rate of 250 ml/min was used. The column was then washed with 100% B for 3 min and then re-equilibrated with 100% A for 6 min. Typically 40 µl injections were used for the analysis. The MS was configured with an Ion Drive Turbo V source; Gas 1 and 2 were set to 40 and 60, respectively; the source temperature to 500 °C and the ion spray voltage to 5500 V. MS, configured with high mass enabled, was used in "Trap" mode to acquire Enhanced Product Ion (EPI) scans for peptide sequencing and in "Triple Quadrupole" mode for Multiple Reaction Monitoring (MRM). Data acquisition and analysis was performed with SCIEX software Analyst 1.6.1 and MultiQuant 3.0. Signature peptides for all the proteins investigated in this work were determined through trial MRM runs. Only the peptide GluFib was used as standard for protein normalisation. The typical work-flow to select the best signature peptides involved the analysis of trial samples in different growth conditions using transitions generated by *in silico* analysis with the open-source Skyline Targeted Mass Spec Environment (MacCoss Lab) (MacLean *et al*, 2010; Abbatiello *et al*, 2013). The identity of candidate peptides was then confirmed by EPI scans. Background proteome of *Anabaena sp. PCC 7120* (http://genome.kazusa.or.jp/cyanobase) was used to check for uniqueness of target peptides. Typically, 3-5 transitions per peptide were used. The final method includes 1-4 peptides per protein for unique identification and quantification. Signature peptides for all the proteins investigated in this work are listed in table 3.

Protein quantification was performed accounting for the intensities of all transitions peaks for all the peptides belonging to a specific protein. The resulted peak area was normalized to the peak intensity of the GluFib peptide standard.

Table 3. Signature peptides for the proteins investigated in this work. *Gene ID, protein ID and corresponding biological function are indicated. Peptides sequences show their position within the corresponding protein in square brackets.*

Gene ID	Protein ID	Biological function	Peptides sequence
Alr1827	IDH	Isocitrate dehydrogenase	K.GPLTTPVGGGIR.S [100, 111]
			R.SLNVALR.Q [112, 118]
			K.LDVIVYR.E [146, 152]
Alr2328	GS	Glutamine synthetase	K.IELIDLK.F [15, 21]
			K.LGVPIEK.H [205, 211]
			R.IPLSGTNPK.A [348, 356]
			K.NIYELSPEELAK.V [399, 410]
Alr4344	GOGAT	Glutamine oxoglutarate aminotransferase	R.FAQVTNPAIDPLR.E [548, 560]
			R.SLSEIIGR.A [1232, 1239]
			K.TLPIVNTDR.T [1310, 1318]
Alr4255	GDH	Glutamate dehydrogenase	R.LDNGDIR.V [66, 72]
			R.TLEGVK.V [227, 232]
Asl2329	IF7A	Glutamine synthetase regulator	SAQELGLPAEELSHYWNPTQGK [29, 50]
Alr4392	NtcA	Nitrogen-responsive regulatory protein	K.TIFFPGDPAER.V [32, 42]
			R.ENSVFGVLSLLTGNK.S [70, 84]
			R.LLGDLR.E [192, 197]
Ar0485	PipX	PII interacting protein	R.LFFLVGNDIK.A [38, 47]
			K.FQPIGR.T [51, 56]
			K.IIAAAR.T [76, 81]
All2319	PII	Nitrogen regulatory protein PII	R.TGEIGDGK.I [82, 89]
			K.IFISPVEQVIR.I [90, 100]
All1440	NifK	Nitrogenase molybdenum-iron protein	R.EALTVNPAK.G [59, 67]

		beta chain	K.AIPEELEIER.G [334, 343]
			R.IGYPLFDR.H [457, 464]
All1554	NifD	Nitrogenase molybdenum-iron protein alpha chain	K.ELIQEVLK.A [14, 21]
			K.LIEELDVLFPLNR.G [135, 147]
			K.IAASLR.E [311, 316]
			K.AELEQDIQDLK.D [144, 154]
All3879	CphA1	Cyanophycin synthetase	R.GITIDIR.S [269, 275]
			R.GSASELITK.G [808, 816]
			R.TPQATK.T [23, 28]
All3880	CphB1	Cyanophycinase	K.VEILDIR.E [90, 96]
			R.DGWLQVLGK.G [232, 240]
			K.GIGVTADVK.D [263, 271]
Alr0573	CphA2	Cyanophycin synthetase 2	R.DAVFVNR.S [521, 527]
			R.DDYNSNIQSLLR.N [534, 545]
			R.FSGVINVSR.V [93, 101]
All3922	ISO	Isoaspartyl dipeptidase	R.GTIGVVALDTYGK.L [178, 190]
			K.LAVGTSTGGK.G [191, 200]
Standard	GluFib	[Glu1]-Fibrinopeptide B, human	EGVNDNEEGFFSAR [0, 13]

Metabolomic analysis

Sample preparation. Strains of *Anabaena sp. PCC 7120* grown in 6-wells plates were harvested by fast filtration, modifying the protocol from (Eisenhut *et al*, 2008). Briefly, cells were fast filtered in the light without any subsequent washing step, using a vacuum filtration system (0.45 µm pore size nitrocellulose filter, 47 mm diameter (Sigma Aldrich)), using stainless-steel stand and funnel (Sartorius). Filters were then transferred to 50 ml tubes and immediately frozen in liquid nitrogen and stored at -80 °C until metabolites extraction. Time between harvesting and metabolic inactivation by freezing was <10 sec. Deep frozen cells were scraped off the nitrocellulose filters using 80% cold methanol (-20 °C). Cells in cold methanol were transferred to 2 ml polypropylene tubes and metabolite extraction was carried out with a TissueLyser II (Qiagen), using tube holders pre-cooled at -20 °C and adding the same volume of acid-washed glass beads (Sigma-Aldrich), for 5 min at 30 Hz. Metabolites were collected after centrifugation for 10 min, 21000 g, 4 °C. Metabolite extraction was repeated twice, the extracts pooled together and centrifuged again to separate cell debris and other immiscible products. Metabolic extracts were then dried by vacuum centrifugation overnight and stored at -80 °C until use.

Sample derivatisation and mass spectrometry. Dried metabolic extracts were reconstituted in 300 µl of water, using L-phenylalanine-d_5 as internal standard (final concentration 2 µg/ml), then vortexed and centrifuged at 16000g for 10 min. Quality control (QC) samples were prepared by mixing 10 µl of the supernatant of each sample, with the analytical batch including 10% QC samples.

Amino acids quantification. 6-aminoquinolyl-N-hydroxysuccinimidyl carbamate was used for derivatization (AccQTag derivatization) according to the manufacturer's manual (AccQTag, Waters Corp). Briefly, 70 µl of borate buffer (pH 8.6) was added to 10 µl sample, followed by the addition of 20 µl AccQTag reagent (in acetonitrile). Samples were then vortexed and heated at 55°C for 10 minutes. 5 µl of each sample were analysed by HPLC-electrospray ionisation/MS-MS using a Shimadzu UFLC XR/AB SCIEX Triple Quad 5500 system, running in multiple reaction monitoring (MRM) via positive ionization mode. The LC-MS method here exploited is based on the one previously described by (Gray *et al*, 2017), with some modifications, as detailed below.

LC method. Mobile phase A: LC-MS grade water with 0.5% formic acid; mobile phase B: LC-MS grade acetonitrile with 0.5% formic acid. Flow rate: 300 µl/min, with the following gradient elution profile: 0.1 min, 4% B; 10 min, 28% B; 10.5 min, 80% B; 11.5 min, 80% B; 12 min, 4% B; 13 min,4% B. An Acquity HSS T3 UPLC column [2.1 mm × 100 mm, 1.8 µm particle size (Waters Corporation, Milford, MA, U.S.A.)] was used to achieve metabolite separation at 45°C.

MS method. The data were acquired through a Sciex QTRAP 5500 MS/MS system [Applied Biosystem (Forster City, CA, USA)], using the following settings: curtain gas, 40 psi; collision gas, medium; ionspray voltage, 5500 V; temperature, 550°C; ion source gas 1 and 2, 40 and 60 psi, respectively. De-clustering, entrance and collision cell exit potentials were set to 30 V, 10 V and 10 V, respectively. Multiple reaction monitoring (MRM) transitions, retention time (RT) and individually optimised collision energy (CE) for each metabolite are listed in supplementary table S1.

2-oxoglutarate (2-OG) quantification. The ion pairing LC method here exploited was adapted from (Michopoulos, 2018), according to the following settings. Mobile phase A: 10 mM tributylamine (TBA) and 15 mM acetic acid in LC-MS grade water; mobile phase B: 80% methanol and 20% isopropanol. Flow rate: 400 µl/min, with the following gradient elution profile: 0 min, 0% B; 0.5 min, 0% B; 4 min, 5% B; 6 min, 5% B; 6.5 min, 20% B; 8.5 min, 20% B; 14 min, 55% B; 15 min, 100% B; 17 min, 100% B; 18 min, 0% B; 21 min 0% B. The method was transferred to XEVO TQ-S (Waters, Wilmslow, U.K.), using an Acquity UPLC system with 45 °C separation temperature.
MS data were acquired according to the following parameters: capillary voltage, 0.8 kV; source offset, 50 V; desolvation temperature, 500°C; source temperature, 150°C; desolvation gas flow, 1000 L/h; cone gas flow, 150 L/h; neutraliser gas, 7.0 bar; collision gas, 0.15 ml/min; cone voltage, 80 V. Data were acquired through an electrospray negative ionisation, focusing only on $[M-H]^-$ ions. Retention time (RT), multiple reaction monitoring (MRM) transitions and individually optimised collision energy (CE) are listed in supplementary table S2.

Data processing. The raw LC-MS data were analysed using Skyline [MacCoss Lab, (Adams *et al*, 2020)]. External dilution curves were used to determine the range for linear response.

Chemicals and reagents. Metabolite standards (Mass Spectrometry Metabolite Library of Standards, MSMLS) were purchased from IROA Technologies (Michigan, MI, U.S.A.). Acetic acid, tributylamine (TBA), L-phenyl-d5-alanine, were obtained from Sigma-Aldrich (Gillingham, U.K.). LC-MS grade water, water with 0.1% formic acid (v/v) and acetonitrile with 0.1% formic acid (v/v) were purchased from Fisher Scientific (Leicester, U.K.). Methanol and isopropanol were purchased from Honeywell (Charlotte, NC, U.S.A.). AccQTag Ultra reagent was purchased from Waters UK.

Statistical analysis

Descriptive statistical analysis was applied for all the data presented in this work. Statistical significance was assessed by one-way analysis of variance (One-way ANOVA) using OriginPro 2018b (v. 9.55) (http://www.originlab.com/). Samples size was at least >4 for all the measurements collected in this work.

Acknowledgments

We acknowledge professor Enrique Flores from the institute of Plant Biochemistry and Photosynthesis, University of Sevilla (Sevilla, Spain), for kindly providing both the *Anabaena sp. PCC 7120* wild-type (WT) and the KO strain for the *amt* gene cluster.

We also acknowledge help and support from Dr. Mark Bennett and Dr. Paul Hitchen with MRM-MS protein quantification, and from Dr. David Malatinszky for setting up high-throughput GS and ammonium quantification assays.
We thank Stephen Rothery (FILM) for help with image analysis also acknowledge the funding from the Wellcome Trust (grant 104931/Z/14/Z) and BBSRC (grant BB/L015129/1) which support the Facility for Imaging by Light Microscopy (FILM) at Imperial College London.

Funding

We acknowledge funding from the BBSRC project BB/N003608/1.

Author's contribution

GP and PJ, conception, design and writing of the manuscript. GP, experiments coordination, sample collection, data collection and analysis. TF, set up the method for MRM protein quantification and sample run. VSK, set up the method for metabolomic analysis and sample run. DG, set up ImageJ macro for microscope analysis. MC, sample preparation for metabolomic analysis. JB, metabolomic analysis coordination. All authors revised the manuscript and approved its final version.

879 **References**

880 Abbatiello SE, Mani DR, Schilling B, MacLean B, Zimmerman LJ, Feng X, Cusack MP, Sedransk N, Hall
881 SC, Addona T, Allen S, Dodder NG, Ghosh M, Held JM, Hedrick V, Inerowicz HD, Jackson A,
882 Keshishian H, Kim JW, Lyssand JS, et al (2013) Design, implementation and multisite evaluation
883 of a system suitability protocol for the quantitative assessment of instrument performance in
884 liquid chromatography-multiple reaction monitoring-MS (LC-MRM-MS). *Mol. Cell. Proteomics*
885 **12:** 2623–2639
886 Adams DG, Bergman B, Nierzwicki-Bauer SA, Duggan PS, Rai AN & Schüßler A (2013) Cyanobacterial-
887 plant symbioses. In *The Prokaryotes: Prokaryotic Biology and Symbiotic Associations* pp 359–
888 400. Springer-Verlag Berlin Heidelberg
889 Adams DG & Duggan PS (2008) Cyanobacteria-bryophyte symbioses. *J. Exp. Bot.* **59:** 1047–1058
890 Available at: https://academic.oup.com/jxb/article-lookup/doi/10.1093/jxb/ern005 [Accessed
891 January 16, 2020]
892 Adams KJ, Pratt B, Bose N, Dubois LG, St. John-Williams L, Perrott KM, Ky K, Kapahi P, Sharma V,
893 Maccoss MJ, Moseley MA, Colton CA, Maclean BX, Schilling B & Thompson JW (2020) Skyline
894 for Small Molecules: A Unifying Software Package for Quantitative Metabolomics. *J. Proteome*
895 *Res.* **19:** 1447–1458 Available at: https://pubmed.ncbi.nlm.nih.gov/31984744/ [Accessed July 6,
896 2020]
897 Andrade SLA & Einsle O (2007) The Amt/Mep/Rh family of ammonium transport proteins (Review).
898 *Mol. Membr. Biol.* **24:** 357–365 Available at:
899 http://www.tandfonline.com/doi/full/10.1080/09687680701388423 [Accessed February 7,
900 2020]
901 Arcondeguy T, Jack R & Merrick M (2001) PII Signal Transduction Proteins, Pivotal Players in
902 Microbial Nitrogen Control. *Microbiol. Mol. Biol. Rev.* **65:** 80–105
903 Backer R, Rokem JS, Ilangumaran G, Lamont J, Praslickova D, Ricci E, Subramanian S & Smith DL
904 (2018) Plant growth-promoting rhizobacteria: Context, mechanisms of action, and roadmap to
905 commercialization of biostimulants for sustainable agriculture. *Front. Plant Sci.* **871:**
906 Bird C & Wyman M (2003) Nitrate/Nitrite Assimilation System of the Marine Picoplanktonic
907 Cyanobacterium Synechococcus sp. Strain WH 8103: Effect of Nitrogen Source and Availability
908 on Gene Expression. *Appl. Environ. Microbiol.* **69:** 7009–7018
909 Böhme H (1998) Regulation of nitrogen fixation in heterocyst-forming cyanobacteria. *Trends Plant*
910 *Sci.* **3:** 346–351
911 Bolay P, Muro-Pastor MI, Florencio FJ & Klähn S (2018) The distinctive regulation of cyanobacterial
912 glutamine synthetase. *Life* **8:**
913 Boogerd FC, Ma H, Bruggeman FJ, Van Heeswijk WC, García-Contreras R, Molenaar D, Krab K &
914 Westerhoff H V. (2011) AmtB-mediated NH3 transport in prokaryotes must be active and as a
915 consequence regulation of transport by GlnK is mandatory to limit futile cycling of NH4+/NH3.
916 *FEBS Lett.* **585:** 23–28
917 Bressler SL & Ahmed SI (1984) Detection of glutamine synthetase activity in marine phytoplankton:
918 optimization of the biosynthetic assay. *Mar. Ecol. Prog. Ser.* **14:** 207–217
919 Burnat M, Herrero A & Flores E (2014) Compartmentalized cyanophycin metabolism in the
920 diazotrophic filaments of a heterocystforming cyanobacterium. *Proc. Natl. Acad. Sci. U. S. A.*
921 **111:** 3823–3828
922 Cameron JC & Pakrasi HB (2010) Essential role of glutathione in acclimation to environmental and
923 redox perturbations in the cyanobacterium Synechocystis sp. PCC 6803. *Plant Physiol.* **154:**
924 1672–1685

925 Cardona T & Magnuson A (2010) Excitation energy transfer to Photosystem I in filaments and
926 heterocysts of Nostoc punctiforme. *Biochim. Biophys. Acta - Bioenerg.* **1797:** 425–433
927 Christensen DG, Xie X, Basisty N, Byrnes J, McSweeney S, Schilling B & Wolfe AJ (2019) Post-
928 translational Protein Acetylation: An elegant mechanism for bacteria to dynamically regulate
929 metabolic functions. *Front. Microbiol.* **10:**
930 Cumino AC, Marcozzi C, Barreiro R & Salerno GL (2007) Carbon cycling in Anabaena sp. PCC 7120.
931 Sucrose synthesis in the heterocysts and possible role in nitrogen fixation. *Plant Physiol.* **143:**
932 1385–1397
933 Eisenhut M, Huege J, Schwarz D, Bauwe H, Kopka J & Hagemann M (2008) Metabolome phenotyping
934 of inorganic carbon limitation in cells of the wild type and photorespiratory mutants of the
935 cyanobacterium Synechocystis sp. strain PCC 6803. *Plant Physiol.* **148:** 2109–2120
936 Ermakova M, Battchikova N, Richaud P, Leino H, Kosourov S, Isojärvi J, Peltier G, Flores E, Cournac L,
937 Allahverdiyeva Y & Aro EM (2014) Heterocyst-specific flavodiiron protein Flv3B enables oxic
938 diazotrophic growth of the filamentous cyanobacterium Anabaena sp. PCC 7120. *Proc. Natl.*
939 *Acad. Sci. U. S. A.* **111:** 11205–11210
940 Flores E & Herrero A (2005) Nitrogen assimilation and nitrogen control in cyanobacteria. In
941 *Biochemical Society Transactions* pp 164–167.
942 Forcada-Nadal A, Llácer JL, Contreras A, Marco-Marín C & Rubio V (2018) The PII-NAGK-PipX-NtcA
943 regulatory axis of cyanobacteria: A tale of changing partners, allosteric effectors and non-
944 covalent interactions. *Front. Mol. Biosci.* **5:**
945 Forchhammer K (2004) Global carbon/nitrogen control by PII signal transduction in cyanobacteria:
946 From signals to targets. *FEMS Microbiol. Rev.* **28:** 319–333
947 Forchhammer K (2008) PII signal transducers: novel functional and structural insights. *Trends*
948 *Microbiol.* **16:** 65–72
949 Forchhammer K & De Marsac NT (1995) Functional analysis of the phosphoprotein P(II) (glnB gene
950 product) in the cyanobacterium Synechococcus sp. strain PCC 7942. *J. Bacteriol.* **177:** 2033–
951 2040
952 Forchhammer K & Selim KA (2019) Carbon/Nitrogen Homeostasis Control in Cyanobacteria. *FEMS*
953 *Microbiol. Rev.*
954 Forchhammer K & Watzer B (2016) Closing a gap in cyanophycin metabolism. *Microbiol. (United*
955 *Kingdom)* **162:** 727–729
956 Galmozzi C V., Saelices L, Florencio FJ & Muro-Pastor MI (2010) Posttranscriptional regulation of
957 glutamine synthetase in the filamentous cyanobacterium Anabaena sp. PCC 7120: Differential
958 expression between vegetative cells and heterocysts. *J. Bacteriol.* **192:** 4701–4711
959 Giordano M (2013) Homeostasis: An underestimated focal point of ecology and evolution. *Plant Sci.*
960 **211:** 92–101
961 Golden JW & Yoon HS (1998) Heterocyst formation in Anabaena. *Curr. Opin. Microbiol.* **1:** 623–629
962 Gray N, Zia R, King A, Patel VC, Wendon J, McPhail MJW, Coen M, Plumb RS, Wilson ID & Nicholson
963 JK (2017) High-Speed Quantitative UPLC-MS Analysis of Multiple Amines in Human Plasma and
964 Serum via Precolumn Derivatization with 6-Aminoquinolyl-N-hydroxysuccinimidyl Carbamate:
965 Application to Acetaminophen-Induced Liver Failure. *Anal. Chem.* **89:** 2478–2487
966 Herrero A, Muro-Pastor AM & Flores E (2001) Nitrogen control in cyanobacteria. *J. Bacteriol.* **183:**
967 411–425
968 Herrero A, Stavans J & Flores E (2016) The multicellular nature of filamentous heterocyst-forming
969 cyanobacteria. *FEMS Microbiol. Rev.* **40:** 831–854
970 Huergo LF & Dixon R (2015) The Emergence of 2-Oxoglutarate as a Master Regulator Metabolite.

Microbiol. Mol. Biol. Rev. **79:** 419–35 Available at: http://www.ncbi.nlm.nih.gov/pubmed/26424716 [Accessed February 10, 2020]

Inomura K, Bragg J & Follows MJ (2017) A quantitative analysis of the direct and indirect costs of nitrogen fixation: A model based on Azotobacter vinelandii. *ISME J.* **11:** 166–175

Ito T, Tokoro M, Hori R, Hemmi H & Yoshimura T (2018) Production of ophthalmic acid using engineered Escherichia coli. *Appl. Environ. Microbiol.* **84:**

Javelle A, Lupo D, Li XD, Merrick M, Chami M, Ripoche P & Winkler FK (2007) Structural and mechanistic aspects of Amt/Rh proteins. *J. Struct. Biol.* **158:** 472–481

Kellar PE & Goldman CR (1979) A comparative study of nitrogen fixation by the Anabaena-Azolla symbiosis and free-living populations of Anabaena spp. in Lake Ngahawa, New Zealand. *Oecologia* **43:** 269–281

Kumar K, Mella-Herrera RA & Golden JW (2010) Cyanobacterial heterocysts. *Cold Spring Harb. Perspect. Biol.* **2:**

Lechno-Yossef S & Nierzwicki-Bauer SA (2005) Azolla-Anabaena Symbiosis. In *Cyanobacteria in Symbiosis* pp 153–178. Kluwer Academic Publishers

Ludewig U (2006) Ion transport versus gas conduction: function of AMT/Rh-type proteins. *Transfus. Clin. Biol.* **13:** 111–116

Ludewig U, Neuhäuser B & Dynowski M (2007) Molecular mechanisms of ammonium transport and accumulation in plants. *FEBS Lett.* **581:** 2301–2308

MacLean B, Tomazela DM, Abbatiello SE, Zhang S, Whiteaker JR, Paulovich AG, Carr SA & MacCoss MJ (2010) Effect of collision energy optimization on the measurement of peptides by selected reaction monitoring (SRM) mass spectrometry. *Anal. Chem.* **82:** 10116–10124

Malatinszky D, Steuer R & Jones PR (2017) A comprehensively curated genome-scale two-cell model for the heterocystous cyanobacterium Anabaena sp. PCC 7120. *Plant Physiol.* **173:** 509–523

Martín-Figueroa E, Navarro F & Florencio FJ (2000) The GS-GOGAT pathway is not operative in the heterocysts. Cloning and expression of glsF gene from the cyanobacterium Anabaena sp. PCC 7120. *FEBS Lett.* **476:** 282–286

Maxwell K & Johnson GN (2000) Chlorophyll fluorescence—a practical guide. *J. Exp. Bot.* **51:** 659–668 Available at: https://academic.oup.com/jxb/article-lookup/doi/10.1093/jexbot/51.345.659 [Accessed December 12, 2019]

Merida A, Candau P & Florencio FJ (1991) Regulation of glutamine synthetase activity in the unicellular cyanobacterium Synechocystis sp. strain PCC 6803 by the nitrogen source: Effect of ammonium. *J. Bacteriol.* **173:** 4095–4100

Messineo L (1966) Modification of the Sakaguchi reaction: Spectrophotometric determination of arginine in proteins without previous hydrolysis. *Arch. Biochem. Biophys.* **117:** 534–540

Michopoulos F (2018) Ion pair chromatography for endogenous metabolites LC-MS analysis in tissue samples following targeted acquisition. In *Methods in Molecular Biology* pp 83–97. Humana Press Inc.

Mo R, Yang M, Chen Z, Cheng Z, Yi X, Li C, He C, Xiong Q, Chen H, Wang Q & Ge F (2015) Acetylome analysis reveals the involvement of lysine acetylation in photosynthesis and carbon metabolism in the model cyanobacterium synechocystis sp. PCC 6803. *J. Proteome Res.* **14:** 1275–1286 Available at: https://pubmed.ncbi.nlm.nih.gov/25621733/ [Accessed July 6, 2020]

Montesinos ML, Herrero A & Flores E (1997) Amino acid transport in taxonomically diverse cyanobacteria and identification of two genes encoding elements of a neutral amino acid permease putatively involved in recapture of leaked hydrophobic amino acids. *J. Bacteriol.* **179:** 853–862

1017 Montesinos ML, Muro-Pastor AM, Herrero A & Flores E (1998) Ammonium/methylammonium
1018 permeases of a cyanobacterium: Identification and analysis of three nitrogen-regulated amt
1019 genes in synechocystis sp. PCC 6803. *J. Biol. Chem.* **273:** 31463–31470
1020 Mullineaux CW, Mariscal V, Nenninger A, Khanum H, Herrero A, Flores E & Adams DG (2008)
1021 Mechanism of intercellular molecular exchange in heterocyst-forming cyanobacteria. *EMBO J.*
1022 **27:** 1299–1308
1023 Muro-Pastor MI, Reyes JC, Florencio FJ, Vespucio A & Florencio FJ (2001) CYANOBACTERIA PERCEIVE
1024 NITROGEN STATUS BY SENSING INTRACELLULAR 2-OXOGLUTARATE LEVELS Downloaded from
1025 JBC Papers in Press Available at: http://www.jbc.org/ [Accessed February 11, 2020]
1026 Nakayasu ES, Burnet MC, Walukiewicz HE, Wilkins CS, Shukla AK, Brooks S, Plutz MJ, Lee BD, Schilling
1027 B, Wolfe AJ, Müller S, Kirby JR, Rao C V., Cort JR & Payne SH (2017) Ancient regulatory role of
1028 lysine acetylation in central metabolism. *MBio* **8:**
1029 Narainsamy K, Farci S, Braun E, Junot C, Cassier-Chauvat C & Chauvat F (2016) Oxidative-stress
1030 detoxification and signalling in cyanobacteria: The crucial glutathione synthesis pathway
1031 supports the production of ergothioneine and ophthalmate. *Mol. Microbiol.* **100:** 15–24
1032 Nicolaisen K, Hahn A & Schleiff E (2009) The cell wall in heterocyst formation by Anabaena sp. PCC
1033 7120. *J. Basic Microbiol.* **49:** 5–24
1034 Nürnberg DJ, Mariscal V, Bornikoel J, Nieves-Morión M, Krauß N, Herrero A, Maldener I, Flores E &
1035 Mullineaux CW (2015) Intercellular diffusion of a fluorescent sucrose analog via the septal
1036 junctions in a filamentous cyanobacterium. *MBio* **6:**
1037 Omata T, Andriesse X & Hirano A (1993) Identification and characterization of a gene cluster
1038 involved in nitrate transport in the cyanobacterium Synechococcus sp. PCC7942. *Mol. Gen.*
1039 *Genet.* **236:** 193–202 Available at: http://www.ncbi.nlm.nih.gov/pubmed/8437564 [Accessed
1040 January 20, 2020]
1041 Orrs J, Keefery LM, Keiml P, Dinh Nguyen$ T, Wellems$ T, Heinriksonl RL & Haselkom$ $$ R (1981)
1042 Purification, Physical Characterization, and NHz-terminal Sequence of Glutamine Synthetase
1043 from the Cyanobacterium Anabaena 7120"
1044 Paz-Yepes J, Merino-Puerto V, Herrero A & Flores E (2008) The amt gene cluster of the heterocyst-
1045 forming cyanobacterium Anabaena sp. strain PCC 7120. *J. Bacteriol.* **190:** 6535–6539
1046 Percival SL & Williams DW (2013) Cyanobacteria. In *Microbiology of Waterborne Diseases:*
1047 *Microbiological Aspects and Risks: Second Edition* pp 79–88. Elsevier Ltd.
1048 Perin G, Bellan A, Segalla A, Meneghesso A, Alboresi A & Morosinotto T (2015) Generation of
1049 random mutants to improve light-use efficiency of Nannochloropsis gaditana cultures for
1050 biofuel production. *Biotechnol. Biofuels* **8:**
1051 Perin G, Yunus IS, Valton M, Alobwede E & Jones PR (2019) Sunlight-driven recycling to increase
1052 nutrient use-efficiency in agriculture. *Algal Res.* **41:** 101554
1053 Picossi S, Montesinos ML, Pernil R, Lichtlé C, Herrero A & Flores E (2005) ABC-type neutral amino
1054 acid permease N-I is required for optimal diazotrophic growth and is repressed in the
1055 heterocysts of Anabaena sp. strain PCC 7120. *Mol. Microbiol.* **57:** 1582–1592
1056 Rascio N & La Rocca N (2013) Biological Nitrogen Fixation. In *Reference Module in Earth Systems and*
1057 *Environmental Sciences* Elsevier Available at:
1058 https://linkinghub.elsevier.com/retrieve/pii/B9780124095489006850 [Accessed January 16,
1059 2020]
1060 Reitzer L (2003) Nitrogen Assimilation and Global Regulation in Escherichia coli . *Annu. Rev.*
1061 *Microbiol.* **57:** 155–176
1062 Rippka R, Deruelles J & Waterbury JB (1979) Generic assignments, strain histories and properties of

pure cultures of cyanobacteria. *J. Gen. Microbiol.* **111:** 1–61

Ritchie RJ (2006) Consistent sets of spectrophotometric chlorophyll equations for acetone, methanol and ethanol solvents. *Photosynth. Res.* **89:** 27–41

Robinson C (2017) Phytoplankton Biogeochemical Cycles. In *Marine Plankton: A Practical Guide to Ecology, Methodology, and Taxonomy*, Castellani C & Edwards M (eds) pp 42–52. Oxford University Press Available at: https://books.google.co.uk/books?id=NuUWDgAAQBAJ&pg=PA47&lpg=PA47&dq=ammonia+the+most+energetically+favorable+AND+source&source=bl&ots=xOjWZgkiLw&sig=ACfU3U2_3N4PK9NlKmgjtVs0EyMkH8nfeA&hl=en&sa=X&ved=2ahUKEwiLt7GAkZfnAhUYRhUIHeDGDa0Q6AEwCXoECAkQAQ#v=onepa [Accessed January 22, 2020]

Sinetova MA, Červený J, Zavřel T & Nedbal L (2012) On the dynamics and constraints of batch culture growth of the cyanobacterium Cyanothece sp. ATCC 51142. *J. Biotechnol.* **162:** 148–155

Singh SP & Montgomery BL (2011) Determining cell shape: Adaptive regulation of cyanobacterial cellular differentiation and morphology. *Trends Microbiol.* **19:** 278–285

Valladares A, Maldener I, Muro-Pastor AM, Flores E & Herrero A (2007) Heterocyst development and diazotrophic metabolism in terminal respiratory oxidase mutants of the cyanobacterium Anabaena sp. strain PCC 7120. *J. Bacteriol.* **189:** 4425–4430

Valladares A, Montesinos ML, Herrero A & Flores E (2002) An ABC-type, high-affinity urea permease identified in cyanobacteria. *Mol. Microbiol.* **43:** 703–715

Valladares A, Rodríguez V, Camargo S, Martínez-Noël GMA, Herrero A & Luque I (2011) Specific role of the cyanobacterial pipX factor in the heterocysts of Anabaena sp. strain PCC 7120. *J. Bacteriol.* **193:** 1172–1182

Wang S, Orabi EA, Baday S, Bernèche S & Lamoureux G (2012) Ammonium Transporters Achieve Charge Transfer by Fragmenting Their Substrate. *J. Am. Chem. Soc.* **134:** 10419–10427 Available at: https://pubs.acs.org/doi/10.1021/ja300129x [Accessed February 7, 2020]

Watzer B, Engelbrecht A, Hauf W, Stahl M, Maldener I & Forchhammer K (2015) Metabolic pathway engineering using the central signal processor PII. *Microb. Cell Fact.* **14:**

Watzer B & Forchhammer K (2018) Cyanophycin synthesis optimizes nitrogen utilization in the unicellular cyanobacterium Synechocystis sp. strain PCC 6803. *Appl. Environ. Microbiol.* **84:**

Watzer B, Spät P, Neumann N, Koch M, Sobotka R, Macek B, Hennrich O & Forchhammer K (2019) The Signal Transduction Protein PII Controls Ammonium, Nitrate and Urea Uptake in Cyanobacteria. *Front. Microbiol.* **10:** Available at: https://www.frontiersin.org/article/10.3389/fmicb.2019.01428/full [Accessed February 3, 2020]

Wellburn AR (1994) The Spectral Determination of Chlorophylls a and b, as well as Total Carotenoids, Using Various Solvents with Spectrophotometers of Different Resolution. *J. Plant Physiol.* **144:** 307–313

Willis RB, Montgomery ME & Allen PR (1996) Improved Method for Manual, Colorimetric Determination of Total Kjeldahl Nitrogen Using Salicylate. *J. Agric. Food Chem.* **44:** 1804–1807 Available at: https://pubs.acs.org/doi/10.1021/jf950522b [Accessed December 10, 2019]

Yakunin AF & Hallenbeck PC (2002) AmtB is necessary for NH4+-induced nitrogenase switch-off and ADP-ribosylation in Rhodobacter capsulatus. *J. Bacteriol.* **184:** 4081–4088

Zhang CC, Zhou CZ, Burnap RL & Peng L (2018) Carbon/Nitrogen Metabolic Balance: Lessons from Cyanobacteria. *Trends Plant Sci.* **23:** 1116–1130